

Identification and Dynamical Properties of Asteroid Families

David Nesvorný

Department of Space Studies, Southwest Research Institute, Boulder

Miroslav Brož

Institute of Astronomy, Charles University, Prague

Valerio Carruba

Department of Mathematics, UNESP, Guaratinguetá

Asteroids formed in a dynamically quiescent disk but their orbits became gravitationally stirred enough by Jupiter to lead to high-speed collisions. As a result, many dozen large asteroids have been disrupted by impacts over the age of the Solar System, producing groups of fragments known as *asteroid families*. Here we explain how the asteroid families are identified, review their current inventory, and discuss how they can be used to get insights into long-term dynamics of main belt asteroids. Electronic tables of the membership for 122 notable families are reported on the Planetary Data System node. See related chapters in this volume for the significance of asteroid families for studies of physics of large scale collisions, collisional history of the main belt, source regions of the near-Earth asteroids, meteorites and dust particles, and space weathering.

1. INTRODUCTION

As witnessed by the heavily cratered surfaces imaged by spacecrafts, the chief geophysical process affecting asteroids is *impacts*. On rare occasions, the impact of a large projectile can be so energetic that the target asteroid is violently torn apart, and the pieces are thrown into space. The sites of such cosmic accidents are filled with debris that gravitationally accumulate into larger conglomerates, and drift away at speeds that are roughly commensurate with the escape speed from the original target body (V_{esc}). Initially, all orbits are similar, because $V_{\text{esc}} \ll V_{\text{orb}}$, where $V_{\text{orb}} \simeq 15\text{-}20 \text{ km s}^{-1}$ is the orbital speed of main belt asteroids. On **longer timescales, however, the orbits are altered by gravitational perturbations from planets**, and the orbital elements of individual bodies start to diverge.

It may therefore seem challenging to identify fragments of a catastrophic collision that happened eons ago. Fortunately, starting with the pioneering work of K. Hirayama (Hirayama, 1918; see also Cimrman, 1917), astronomers have developed various methods to deal with this issue (Section 2). Roughly speaking, these methods consist in a transformation that brings the **orbital elements at the observed epoch to a standard**, called the *proper elements* (Knežević et al., 2002), that is unchanging in time (or, at least, would be unchanging if chaotic dynamics, non-gravitational forces, and other perturbations could be ignored). Thus, ideally, **daughter fragments produced by breakup of a parent asteroid will appear as a group in space of the proper elements even gigayears after the original collision**. These groups are called asteroid families, or *dynamical families* to emphasize that they have been identified

from **dynamical considerations**.

Telescopic surveys such as the Sloan Digital Sky Survey (SDSS), Wide-field Infrared Survey Explorer (WISE) and AKARI All-Sky Survey provide a wealth of data on physical properties of the main belt asteroids (Ivezić et al., 2001; Mainzer et al., 2011; Usui et al., 2013). They have been used to cross-link the color and albedo measurements with the lists of dynamical families, in much the same way the spectroscopic and taxonomic data have previously been applied to this purpose (see Cellino et al., 2002 for a review). This work is useful to physically characterize the asteroid families (see chapter by Masiero et al. in this volume), including cases where two or more dynamical families overlap, and identify distant “halo” family members that would otherwise be confused with the local background (e.g., Brož and Morbidelli, 2013). Given that the SDSS and WISE catalogs now contain data for over 100,000 unique asteroids, it has also become practical to conduct search for families in extended space, where the color and/or albedo data are taken into account simultaneously with the orbital elements (e.g., Parker et al., 2008; Masiero et al., 2013; Carruba et al., 2013a).

The physical data can be used to identify *interlopers*. The problem of interlopers arises because the clustering criterion applied to identify the dynamical families is only a rough expression of the true membership. Unrelated asteroids that just happen to have nearby values of proper elements will be grouped together with the true members, and will thus appear in the lists of dynamical families obtained from the proper elements (e.g., Migliorini et al., 1995). These interlopers, especially the large ones, intro-

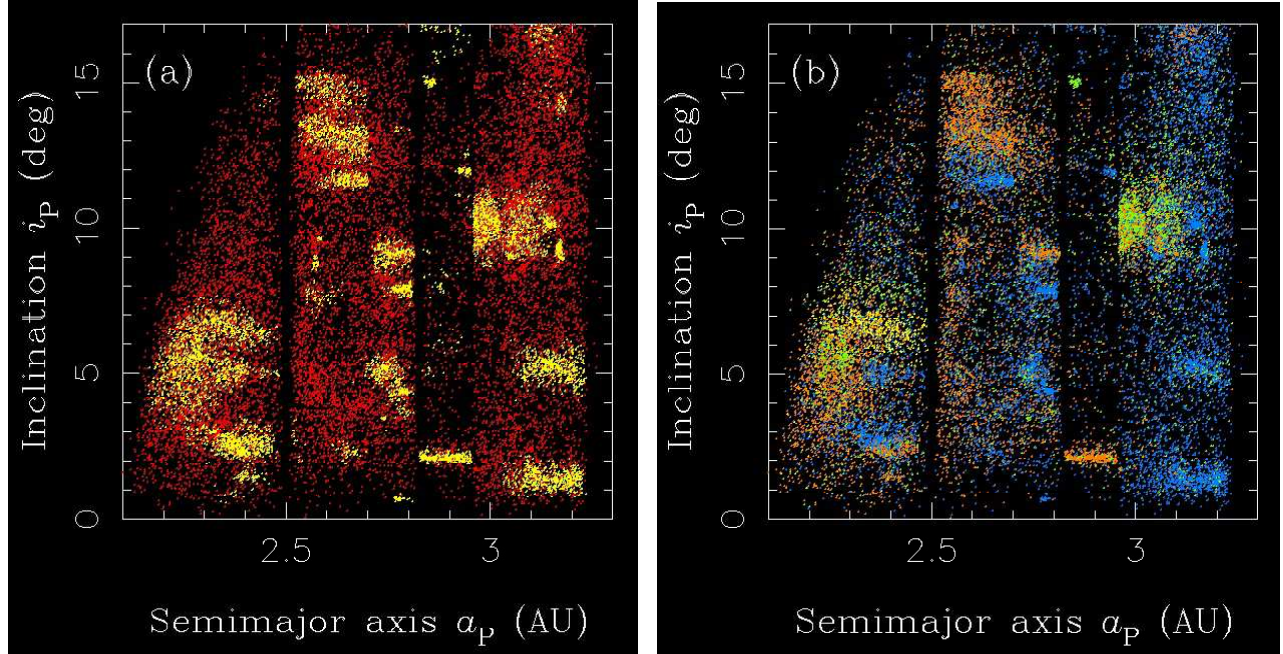


Fig. 1.— (a) Clustering algorithm applied to the asteroid belt separates dynamical families (yellow) from the background (red). (b) Variation in reflectance properties of main belt asteroids. Here we plot $\simeq 25,000$ asteroids that were observed by both SDSS and WISE. The color code was chosen to highlight the albedo/color contrast of different families.

duce ambiguity in the interpretation of impact conditions that produced individual families, and in the implications of these studies for asteroid interiors (cf. Michel et al., 2003; Nesvorný et al., 2006a). Here we discuss how large interlopers and true largest members in families can be found by applying the “V-shape” criterion, which is based on the notion that large fragments are ejected at low speeds, and have less mobility due to the Yarkovsky effect (Section 4).

Based on the synthesis of asteroid families extracted from recent publications (Mothé-Diniz et al., 2005; Nesvorný et al., 2005; Gil-Hutton, 2006; Parker et al., 2008; Nesvorný, 2010, 2012; Novaković et al., 2011; Brož et al., 2013; Masiero et al., 2011, 2013; Carruba et al., 2013a; Miliani et al., 2014), we attempt to build a consensus that could serve as a starting point for future studies. We classify the asteroid families into *notable* cases (those that have a high statistical significance, and are thus real, and/or are notable for other reasons) and *candidate* families (less interesting cases where the statistical significance is low or cannot currently be established). The distinction between notable and candidate families is somewhat arbitrary, and will intentionally be left strictly undefined, because that is the nature of things. We expect that many candidate families will be confirmed with more data, and that a few notable families may fall into oblivion. The lists of notable families are being made available at the Planetary Data System (PDS) node, and are discussed in Section 7.

A new and exciting development in the past decade was the detection of several asteroid families with very young formation ages. For example, the Karin family was shown to have formed only 5.8 ± 0.2 m.y. ago (Nesvorný et al.,

2002a). These cases are important, because various collisional and dynamical processes had little time to act on these families to alter their properties. The young families have thus attracted much attention from scientists studying impact physics, space weathering, debris disks, etc. As we explain in Section 3, the age of a young family can be determined by numerically integrating the orbits of its members backward in time and demonstrating that they converge to each other at some specific time in the past. This is the time of a breakup, and the family age, t_{age} , is the time elapsed from the breakup event.

The method of backward integration of orbits only works for the families with $t_{\text{age}} \lesssim 10$ m.y. This is because dynamics of main-belt asteroids on longer timescales is governed by chaos, encounters with (1) Ceres and other large asteroids, and non-gravitational forces. A complementary statistical method for the estimation of family age has been developed in Vokrouhlický et al. (2006a,b). The method tracks, in detail, how the family structure in semimajor axis changes over time as the family members drift away by the Yarkovsky effect (Section 5). The semimajor axis spread of an older family will generally be greater than that of a younger family. A compilation of formation ages of the asteroid families can be used to constrain how the population of the asteroid belt collisionally evolved over time (e.g., Bottke et al., 2005a,b; Cibulková et al., 2014), and how asteroid surfaces age by space weathering (chapter by Brunetto et al. in this volume).

2. IDENTIFICATION METHOD

Here we discuss the standard method to identify asteroid families. This method consists of the (1) computation of proper elements, or other elements unchanging with time, for asteroids with well-known orbits, (2) identification of concentrations or groups of asteroids in proper element space, and (3) establishing the statistical significance of identified groups. These steps are discussed in Sections 2.1, 2.2 and 2.3. In Section 2.4, we examine the “overlap problem” where two or more families overlap in proper element space, and need to be separated. For this it is useful to consider families in *extended* space with physical data being included in addition to the proper elements. The search in extended space can also lead to the identification of new families (Section 2.5). Very young families ($t_{\text{age}} \lesssim 1$ m.y.), for which the member orbits have not had time to differentially precess away from each other, can also be identified as groups in space of the *osculating* orbital elements (Section 2.6).

2.1 PROPER ELEMENTS

The ejection speeds of sizable fragments produced by collisional breakups of main belt asteroids are generally much smaller than their orbital speeds. The fragments will therefore initially cluster near the original orbit of their parent body, and will appear as such if the subsequent effects of planetary perturbations are removed by projecting orbits into space of proper elements. The three most useful proper elements are: the proper semimajor axis (a_P), the proper eccentricity (e_P), and the proper inclination (i_P). They are close equivalents of their osculating element counterparts in that they define the size, elongation and tilt of orbits (see Note 1 in Section 9).

The definition of proper elements as quasi-integrals of asteroid motion, and the methods used to compute them, were explained in the Asteroids III book (Knežević et al., 2002). As these definitions and methods have not changed much, we do not discuss them here in detail. In brief, the proper elements are obtained from the instantaneous osculating orbital elements by removing periodic oscillations produced by gravitational perturbations of planets. This can be done analytically, using perturbation theory (Milani and Knežević, 1990, 1994), or numerically, by integrating the orbits and applying the Fourier analysis (Knežević and Milani, 2000; Knežević et al., 2002) (Note 2).

The computation of analytic proper elements is relatively CPU inexpensive. They are made publicly available by A. Milani for both numbered and unnumbered multi-opposition asteroids at the AstDyS node (Note 3). The analytic proper elements lose precision for highly-inclined orbits, because the expansion of the gravitational potential used to calculate them has poor convergence for high inclinations. The more-precise synthetic proper elements (precision generally at least 3 times better than that of analytic elements), on the other hand, require a much larger CPU

investment, and are only made available at the AstDyS node for the numbered asteroids.

2.2 CLUSTERING ALGORITHM

When these methods are applied to the asteroid belt, things are brought into focus with dozens of obvious clumps, asteroid families, emerging from the background (Figure 1a). To identify an asteroid family, researchers apply a clustering algorithm to the distribution of asteroids in (a_P, e_P, i_P) space. The most commonly used algorithm is the Hierarchical Clustering Method (HCM; Zappalà et al., 1990) (Note 4), which defines a cutoff distance, d_{cut} , and requires that the length of the link between two neighboring orbits clustered by the algorithm is $d = d(a_P, e_P, i_P) < d_{\text{cut}}$. A common definition of distance is $d^2 \equiv (n a_P)^2 (k_a (\delta a_P / a_P)^2 + k_e (\delta e_P)^2 + k_i (\delta i_P)^2)$, where n is the orbital frequency, $(\delta a_P, \delta e_P, \delta \sin i_P)$ is the separation vector between orbits in 3D space of proper elements, and (k_a, k_e, k_i) are coefficients of the order of unity.

The main advantage of the HCM over other methods is that there is no strong assumption built into the HCM about the shape of an asteroid family in proper element space. This is because the chain created by linking nearby orbits can track down family members even if their orbits dynamically evolved to produce an unusual overall shape. A prime example of this is the case of the Koronis family which is split into two parts by the secular resonance $g + 2g_5 - 3g_6 = 0$ at ≈ 2.92 AU, where g is the apsidal frequency of an asteroid, and g_5 and g_6 are the 5th and 6th apsidal frequencies of the planetary system. The part of the Koronis family with $a_P > 2.92$ AU has larger eccentricity than the part with $a_P < 2.92$ AU, because family members drifting by the Yarkovsky effect from $a_P < 2.92$ AU have their eccentricities increased by interacting with the $g + 2g_5 - 3g_6 = 0$ resonance (Bottke et al., 2001).

The main disadvantage of the standard HCM, which becomes increasingly difficult to overcome with inclusion of numerous small asteroids in the new catalogs, is the problem of *chaining*. This problem arises because small fragments are typically ejected at higher speeds and have larger mobility due to the Yarkovsky effect. They therefore spread more, tend to be distributed more homogeneously throughout the main belt, and create bridges between different families if a single (large) value of d_{cut} is used. Clearly, d_{cut} should be set proportional to the asteroid size, or inversely proportional to the absolute magnitude H . Expressing this dependence, however, adds additional parameters to the HCM and makes the whole identification procedure more complex. Therefore, in reality, it is preferred to bypass the problem of chaining by artificial means (e.g., cuts in proper element space applied to deal with individual cases), or the proportionality is approximated by a two-step method with different cutoffs for small and large bodies (Milani et al., 2014).

A tricky part of the HCM algorithm is the choice of the cutoff distance. If the value of d_{cut} is too small, many

dispersed but real families will remain unnoticed and large families will artificially be split into parts. If the value is too large, the algorithm will clump different families together, and will identify irrelevant clumps produced by random fluctuations. While many asteroid families can be identified for a wide range of d_{cut} values, and are real beyond doubt, some cases require a specific choice of d_{cut} and can potentially be confused with random fluctuations. Clearly, the *statistical significance* of the identified groups, or their insignificance, needs to be established before proceeding further.

2.3 STATISTICAL SIGNIFICANCE

To make reasonably sure that families identified from the HCM are real one can opt for a conservative choice of d_{cut} . This can be done, for example, by collecting asteroids in a given region of proper element space and redistributing them randomly in that region. The HCM applied to this artificial distribution will reveal that the largest identified group with given d_{cut} contains $N^*(d_{\text{cut}})$ members. Now, this procedure can be repeated, say, one thousand times, recording the largest $N^*(d_{\text{cut}})$ obtained from these trials. We can then be 99% confident that random fluctuations cannot produce groups with more than $N^*(d_{\text{cut}})$ members (this conservative estimate includes a 99% confidence interval computed by the Wilson score interval approximation). Any group identified in the *real* distribution with $N > N^*(d_{\text{cut}})$ members is therefore reasonably likely to be real. Higher confidence levels can be achieved by increasing the sample size.

This basic concept, and various modifications of it, is known as the Quasi Random Level (QRL; Zappalà et al., 1994). In the ideal world, the QRL would be the ultimate solution to the family identification problem: just choose d_{cut} and pick up all clumps with more than $N > N^*(d_{\text{cut}})$; those clumps are real. Then, there is the real world. First, the number density in proper element space is variable due to the primordial sculpting of the main belt and resonances (e.g., Minton and Malhotra, 2009). Applying a *global* QRL value in (parts of) the main belt may therefore lead to unsatisfactory results. Second, families do not live in isolation but are frequently close to each other, overlap, and/or are surrounded by empty regions. This introduces an ambiguity in the QRL definition, because it is not clear *a priori* what region in (a_p, e_p, i_p) space should be considered to define the *local* QRL in the first place. Results may depend on this choice.

In practice, the first choice made is often the minimum number of group members, N_{\min} , that is considered to be interesting. Then, the cutoff distance d_{cut} in some local region in (a_p, e_p, i_p) is defined such that groups of $N > N_{\min}$ members cannot be produced with d_{cut} by random fluctuations. All groups with $N > N_{\min}$ are then treated as meaningful asteroid families. Different researchers made different choices: $N_{\min} = 5$ in Zappalà et al. (1990), $N_{\min} = 100$ in Parker et al. (2008), and $N_{\min} = 10\text{-}20$ in most other publications. The two disad-

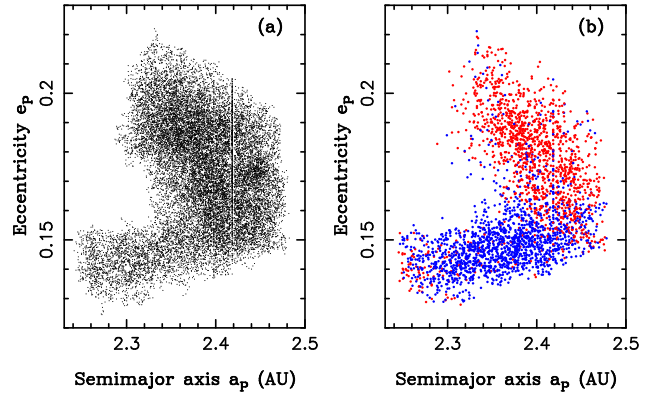


Fig. 2.— The Nysa-Polana complex. (a) The HCM applied to this region of the inner main belt reveals a major concentration of asteroids with $2.25 < a_p < 2.48$ AU and $0.13 < e_p < 0.22$. The shape of the concentration in the (a_p, e_p) projection is unusual and difficult to interpret. (b) The WISE albedos of members of the Nysa-Polana complex: black for $p_V < 0.15$ and gray for $p_V > 0.15$. It becomes clear with the albedo information that the Nysa-Polana complex is two overlapping groups with distinct albedos. Furthermore, based on the V-shape criterion (Section 4), the low-albedo group is found to consist of two asteroid families (the Polana and Eulalia families; Walsh et al., 2013). The vertical feature at $a_p \simeq 2.42$ AU is the 1:2 mean motion resonance with Mars.

vantages of this method are that: meaningful asteroid families with $N < N_{\min}$ members are explicitly avoided, and $d_{\text{cut}}(N_{\min})$ depends on the population density in proper element space and must be recomputed when a new classification is attempted from ever-growing catalogs.

Another approach to this problem is to identify all groups, even if they have only a few members, and establish their statistical significance *a posteriori*. Those that are judged to be insignificant are subsequently discarded and do not appear in the final lists. To determine the statistical significance of a group, one can generate mock distributions and apply the HCM to them. For example, the high statistical significance of the Karin family, which is embedded in the much larger Koronis family, can be demonstrated by generating thousand orbital distributions corresponding to the Koronis family, and applying the HCM to each one (Nesvorný et al., 2002a). With $d_{\text{cut}} = 10 \text{ m s}^{-1}$, no concentrations in this input can be found containing more than a few dozen members, while the Karin family currently has 541 known members. Therefore, the Karin family is significant at a greater than the 99% level (again including a 99% confidence interval of the estimate). A systematic application of this or similar statistical arguments can be quite laborious if many borderline cases need to be resolved.

2.4 OVERLAP PROBLEM AND INTERLOPERS

The overlap between different families has become more of a problem with a progressively larger share being taken in the proper element catalogs by small, km and sub-km

size asteroids. This is because small fragments are generally launched at higher speeds, and are therefore initially spread in a larger volume in (a_P, e_P, i_P) space. Mainly, however, the problem is caused by the larger mobility of small fragments due to the Yarkovsky effect. For example, the mean drift rate of a diameter $D = 1$ km main belt asteroid is estimated to be $\simeq 10^{-4}$ AU/m.y. (Bottke et al., 2006). The km-size members of a 1-g.y. old family are therefore expected to be dispersed over $\simeq 0.2$ AU (the additional factor of two accounts here for fragments having different spin orientations, and thus $da/dt < 0$ or $da/dt > 0$), which is roughly 1/5 of the extension of the whole main belt. In addition, drifting asteroids encounter orbital resonances and can be dispersed by them in e_P and i_P as well.

A good illustration of this is the case of the Flora and Vesta families in the inner main belt. To separate these families from each other down to their smallest members, the scope of the HCM can be restricted by an artificial cut in proper element space. Alternatively, one can first apply the HCM to the distribution of large members, thus identifying the core of each family, and then proceeding by trying to “attach” the small members to the core. This second step must use a lower d_{cut} value than the first step to account for the denser population of smaller asteroids. In practice, this has been done by applying an absolute magnitude cutoff, H^* , with $H < H^*$ for the core and $H > H^*$ for the rest. In the low- i portion of the inner main belt, where the Flora and Vesta families reside, Milani et al. (2014) opted to use $H^* = 15$, and identified cores of families with $N_{\min} = 17$ and $d_{\text{cut}} = 60 \text{ m s}^{-1}$, and small members with $N_{\min} = 42$ and $d_{\text{cut}} = 40 \text{ m s}^{-1}$.

Another solution to the overlap problem is to consider the *physical* properties of asteroids. Previously, the spectroscopic observations of members of dynamical families have been used to: (1) establish the physical homogeneity of asteroid families (the difference between physical properties of members of the same family tends to be smaller than the differences between physical properties of different families), and (2) identify large interlopers (asteroids classified as family members based on proper elements but having spectroscopic properties distinct from the bulk of the family). With the color and albedo data from the SDSS and WISE (Note 5), the physical homogeneity of asteroid families has been demonstrated to hold down to the smallest observable members (Ivezic et al., 2001; Parker et al., 2008; see Figure 1b). A straightforward implication of this result is that the interior of each disrupted body was (relatively) homogeneous, at least on a scale comparable to the size of the observed fragments ($\sim 1\text{-}100$ km) (Note 6).

The physical homogeneity of asteroid families can be used to identify *interlopers* as those members of a dynamical family that have color and/or albedo significantly distinct from the rest of the family. The number density of apparent color/albedo interlopers in a family can then be compared with the number density of the same color/albedo asteroids in the immediate neighborhood of the family. Similar densities are expected if the identified bodies are actual

interlopers in the family. If, on the other hand, the density of color/albedo outliers in the family is found to be substantially higher than in the background, this may help to rule out the interloper premise, and instead indicate that: (i) the disrupted parent body may have been heterogeneous, or (ii) we are looking at two or more overlapping dynamical families with distinct color/albedo properties. Finally, as for (ii), it is useful to verify whether the family members with different color/albedo properties also have different proper element distributions, as expected if breakups happened in two (slightly) different locations in proper element space (e.g., the Nysa-Polana complex; see Figure 2).

2.5 FAMILIES IN EXTENDED SPACE

Another useful strategy is to include the color and/or albedo information *directly* in the clustering algorithm. This can be done by first separating the main belt into two (or more) populations according to their color and albedo properties. For example, asteroids in the S-complex can be separated from those in the C/X-complex based on the SDSS colors (Nesvorný et al. 2005), and the high-albedo asteroids can be separated from the low-albedo asteroids based on the albedo measurements of WISE (Masiero et al., 2013). The HCM is then applied to these populations separately. This method is capable of identifying small/dispersed S-complex families in the C/X-type background, and vice-versa, or low-albedo families in the high-albedo background, and vice-versa. It can also be useful to characterize the so-called family “halos” (Section 6.4).

A more general method for including the color/albedo information in the clustering algorithm consists in the application of the HCM in space of increased dimension (e.g., Parker et al. 2008; Carruba et al., 2013a). When considering the proper elements and SDSS colors, the distance in 5D can be defined as $d_2^2 \equiv d^2 + n^2 a_P^2 (k_1(\delta C_1)^2 + k_2(\delta C_2)^2)$, where d is the distance in 3D space of proper elements defined in Section 2.2, C_1 and C_2 are two diagnostic colors defined from the SDSS (Ivezic et al., 2001; Nesvorný et al., 2005), and k_1 and k_2 are coefficients whose magnitude is set to provide a good balance between the orbital and color dimensions (e.g., Nesvorný et al., 2006b). Similarly, we can define $d_3^2 \equiv d^2 + n^2 a_P^2 k_p (\delta p_V)^2$ (in 4D) and $d_4^2 \equiv d_2^2 + n^2 a_P^2 k_p (\delta p_V)^2$ (in 6D) to include the measurements of albedo p_V from WISE. The d_4 metric applies the strictest criteria on the family membership, because it requires that the family members have similar proper elements, similar colors, and similar albedos. Note, however, that this metric can only be applied to a reduced set of main belt asteroids for which the proper elements, colors and albedos are *simultaneously* available (presently $\simeq 25,000$; Figure 1b).

2.6 VERY YOUNG FAMILIES IN ORBITAL ELEMENT SPACE

Short after family’s creation, when the mutual gravity effects among individual fragments cease to be important, the

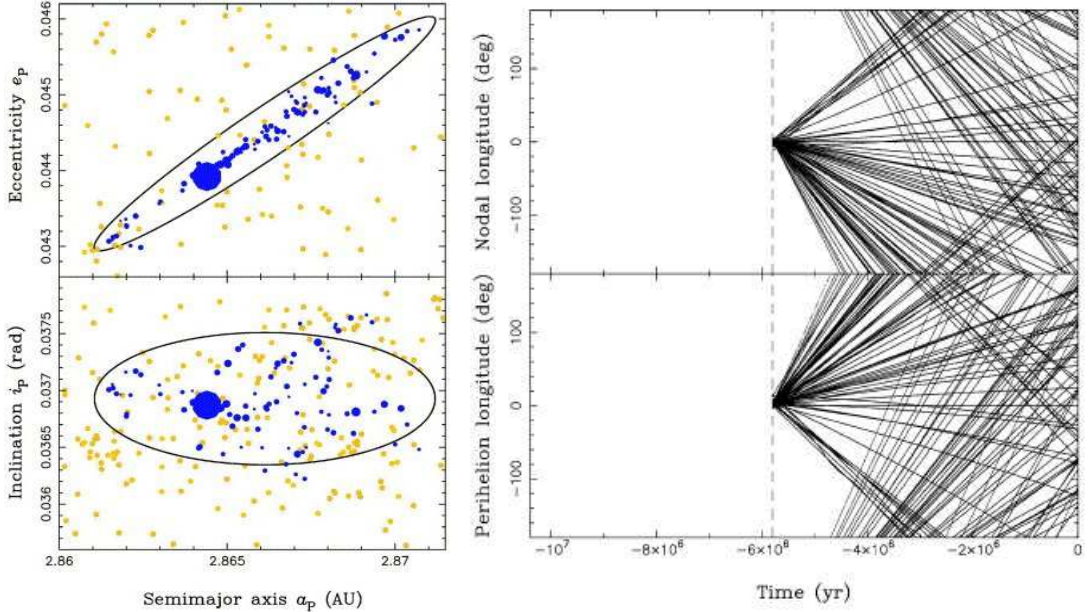


Fig. 3.— **Left panels:** Proper elements of members of the Karin family. The size of each dark symbol is proportional to the diameter of a family member. Light gray dots indicate background bodies near the Koronis family. The black ellipses show the proper orbital elements of test bodies launched at 15 m s^{-1} from $a_P = 2.8661 \text{ AU}$, $e_P = 0.04449$ and $i_P = 0.03692$, assuming that $f = 30^\circ$ and $\omega + f = 45^\circ$, where f and ω are the true anomaly and perihelion argument of the disrupted body at the time of the family-forming collision. **Right panels:** The convergence of angles at 5.8 m.y. ago demonstrates that the Karin family was created by a parent asteroid breakup at that time. The plot shows past orbital histories of ninety members of the Karin family: (top) the proper nodal longitude, and (bottom) the proper perihelion longitude. Values of these angles relative to (832) Karin are shown. At $t = 5.8$ m.y. (broken vertical line), the nodal longitudes and perihelion arguments of all ninety asteroids become nearly the same, as expected if these bodies had initially nearly the same orbits. Adapted from Nesvorný and Bottke (2004).

fragments will separate from each other and find themselves moving on heliocentric orbits. Initially, they will have very tightly clustered orbits with nearly the same values of the osculating orbital angles Ω , ϖ and λ , where Ω is the nodal longitude, ϖ is the apsidal longitude, and λ is the mean longitude. The debris cloud will be subsequently dispersed by the (i) *Keplerian shear* (different fragments are ejected with different velocity vectors, have slightly different values of the semimajor axis, and therefore different orbital periods) and (ii) *differential precession* of orbits produced by planetary perturbations.

As for (i), the fragments will become fully dispersed along an orbit on a timescale $T_n = \pi/(a\partial n/\partial a)(V_{\text{orb}}/\delta V) = (P/3)(V_{\text{orb}}/\delta V)$, where $P = 2\text{-}4 \text{ yr}$ is the orbital period and δV is the ejection speed. With $\delta V = 1\text{-}100 \text{ m s}^{-1}$, this gives $T_n = 300\text{-}30,000 \text{ yr}$. Therefore, the dispersal of fragments along the orbit is relatively fast, and the clustering in λ is *not* expected if a family is older than a few tens of thousand years.

The dispersal of Ω and ϖ occurs on a time scale $T_f = \pi/(a\partial f/\partial a)(V_{\text{orb}}/\delta V)$, where the frequency $f = s$ or g . For example, $\partial s/\partial a = -70 \text{ arcsec yr}^{-1} \text{ AU}^{-1}$ and $\partial g/\partial a = 94 \text{ arcsec yr}^{-1} \text{ AU}^{-1}$ for the Karin family ($a \simeq 2.865 \text{ AU}$). With $\delta V = 15 \text{ m s}^{-1}$ (Nesvorný et al., 2006a) and $V_{\text{orb}} = 17.7 \text{ km s}^{-1}$, this gives $T_s = 3.8 \text{ m.y.}$ and $T_g = 2.8 \text{ m.y.}$ Since $t_{\text{age}} > T_s$ and $t_{\text{age}} > T_g$ in this

case, the distribution of Ω and ϖ for the Karin family is not expected to be clustered at the present time (Figure 3). Conversely, the clustering of Ω and ϖ would be expected for families with $t_{\text{age}} \lesssim 1 \text{ m.y.}$

This expectation leads to the possibility that the families with $t_{\text{age}} \lesssim 1 \text{ m.y.}$ could be detected in the catalogs of osculating orbital elements (Marsden, 1980; Bowell et al., 1994), where they should show up as clusters in 5D space of a , e , i , ϖ and Ω . The search in 5D space of the osculating orbital elements can be performed with the HCM method and metric $d_5^2 = d^2 + (na)^2(k_\Omega(\delta\Omega)^2 + k_\varpi(\delta\varpi)^2)$, where $d = d(a, e, i)$ was defined in Section 2.2, and k_Ω and k_ϖ new coefficients. [Different metric functions were studied by Rožek et al. (2011), who also pointed out that using the *mean* elements, instead of the osculating ones, can lead to more reliable results.]

This method was first successfully used in practice for the identification of the Datura family (Nesvorný et al., 2006c), and soon after for the discovery of the asteroid pairs (Vokrouhlický and Nesvorný, 2008). The Datura family now consists of 15 known members ranging in size from $\simeq 10\text{-km-diameter object}$ (1270) Datura to sub-km fragments. They have Ω and ϖ clustered to within a few degrees near 98° and 357° , respectively. The age of the Datura family is only $530 \pm 20 \text{ k.y.}$, as estimated from the backward integration of orbits (Vokrouhlický et al., 2009). Table 1

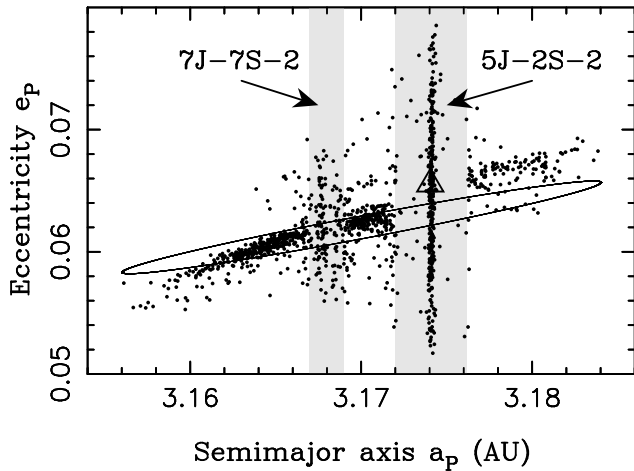


Fig. 4.— The Veritas family. Here we plot the proper elements of 1294 members of the Veritas family identified from a new catalog (August 2014). (490) Veritas itself is marked by a triangle. The gray vertical strips indicate two three-body resonances which act to diffuse the orbits of family members in e_P . The black ellipse shows the orbital elements of test bodies launched at $\delta V = 35 \text{ m s}^{-1}$ from $a_P = 3.17 \text{ AU}$ and $e_P = 0.0062$, assuming that $f = 30^\circ$, where f is the true anomaly of the disrupted body at the time of the family-forming collision.

reports other notable cases of families with $t_{\text{age}} < 1 \text{ m.y.}$

3. DETECTION OF RECENT BREAKUPS

The detection of families with very young formation ages was one of the highlights of asteroid research in the past decade. A poster child of this exciting development is the Karin family, part of the larger Koronis family, that was shown to have formed only $5.8 \pm 0.2 \text{ m.y.}$ ago (Nesvorný et al., 2002a). The Karin family was identified by the traditional means, using the HCM on proper elements. The diagonal shape of this family in the (a_P, e_P) projection is a telltale signature of a recent breakup, because this initial shape is expected if a breakup occurs near the perihelion of the parent body orbit (Figure 3). In this case, the tilt α of the family shape in the (a_P, e_P) projection is expected to be, and indeed is in the case of the Karin family, $\tan \alpha = \Delta e_P / (\Delta a_P / a_P) = (1 - e_P) = 0.956$. Thus, $\alpha \approx 45^\circ$. All other known families, with an exception of the similarly-young Veritas family, have $\alpha \sim 0$ (i.e., are nearly horizontal features in a_P, e_P). This is because these families are old and their original shape was stretched in a_P by the Yarkovsky effect (e.g., Dell’Oro et al., 2004).

The age of the Karin family has been established by numerically integrating the orbits of identified members back in time in an attempt to identify their past convergence (Figure 3). The past convergence is expected because the spread of the Karin family in a_P, e_P, i_P indicates that the ejection speeds of observed fragments were only $\lesssim 15 \text{ m s}^{-1}$. These low speeds imply a very tight *initial* distribution (to within $\approx 1^\circ$) of λ, ϖ and Ω . The backward integration showed that the convergence occurred at 5.8 ± 0.2

m.y. ago. In addition, the past convergence improved, with ϖ and Ω of all member orbits converging to within a degree, if the backward integration included the Yarkovsky drift (Nesvorný and Bottke, 2004). This was used to measure the rate of the Yarkovsky drift for individual members of the family, determine their obliquities, and pin down the age of the Karin family to $t_{\text{age}} = 5.75 \pm 0.05 \text{ m.y.}$

The method of backward integration of orbits was applied to several families (Nesvorný et al., 2002a, 2003, 2008b; Novaković et al., 2010, 2012a,b, 2014; Table 1; some of these results will need to be verified). One of the interesting results that emerged from these studies is a possible relationship between the young families and Main Belt Comets (MBCs; see chapter by Jewitt et al. in this volume). For example, (7968) P/133 Elst-Pizzaro can be linked to the Beagle family ($t_{\text{age}} \sim 10 \text{ m.y.}$; Nesvorný et al., 2008b), and (300163) P/2006 VW139 and P/2012 F5 (Gibbs) can be linked to small families that probably formed within the past 10 m.y. (Novaković et al., 2012a, 2014). If this relationship is confirmed by future studies, this can help us to understand how the MBCs are “activated”.

Another notable case of a recent breakup is the Veritas family (Figure 4). It has previously been hypothesized that the Veritas family is $< 50 \text{ m.y.}$ old (Milani and Farinella 1994). This claim was based on the argument that the largest member of the dynamical family, (490) Veritas, has chaotic dynamics and would be expected to diffuse away in e_P from the rest of the family, if the family were older than $\sim 50 \text{ m.y.}$ [Note, however, that recent impact modeling may indicate that (490) Veritas is not a true member of the Veritas family (e.g., Michel et al., 2011).] A backward integration of orbits confirmed the young age, and showed that the Veritas family formed only $8.3 \pm 0.5 \text{ m.y.}$ ago (Nesvorný et al., 2003).

A similarly young age was later obtained by an independent method, known as the “chaotic chronology”, based on tracking the evolution of orbits in one of the diffusive resonances that intersect the Veritas family (Tsiganis et al., 2007, see also Knežević and Pavlović, 2002). Tsiganis et al. (2007) considered the chaotic diffusion of the Veritas family members in the 5J-2S-2 three-body resonance at 3.174 AU (Nesvorný and Morbidelli, 1999). Based on numerical integrations of chaotic orbits they estimated that the observed spread in the 5J-2S-2 resonance can be obtained for $t_{\text{age}} = 8.7 \pm 1.7 \text{ m.y.}$ Interestingly, the Veritas family is also intersected by the 7J-7S-2 resonance at 3.168 AU. The observed distribution of eccentricities in this resonance is rather wide and cannot be explained by normal diffusion over the estimated age (the 7J-7S-2 resonance is ~ 100 times less diffusive than the 5J-2S-2 resonance). Perhaps the problem is with the HCM chaining, discussed in Section 2.2, which links unrelated asteroids in the 7J-7S-2 resonance, or the dynamical modeling is missing some important ingredient. Novaković et al. (2010) applied the method of chaotic chronology to the Theobalda family and found that the estimated age is consistent with that obtained from a backward integration of the regular or-

Table 1: Recently formed asteroid families.

Family/Pair	t_{age}	References	Notes
(832) Karin	5.75 ± 0.05 m.y.	Ne02,NB04	2.1° dust band
(158) Koronis(2)	10-15 m.y.	MH09	near (832) Karin
(490) Veritas	8.3 ± 0.5 m.y.	Ne03,F06,T07	9.3° band, late Miocene dust shower
(656) Beagle	~ 10 m.y.	Ne08	1.4° band, member Elst-Pizzaro?
(778) Theobalda	6.9 ± 2.3 m.y.	No10	t_{age} needs to be confirmed
(1270) Datura	530 ± 20 k.y.	Ne06,V09	identified in 5D, E/F dust band?
(2384) Schulhof	780 ± 100 k.y.	VN11	secondary breakup event?
(4652) Iannini	$\lesssim 5$ m.y.	Ne03,W08	chaotic dynamics
(5438) Lorre	1.9 ± 0.3 m.y.	No12a	$i_P \simeq 28^\circ$
(14627) Emilkowalski	220 ± 30 k.y.	NV06	only 3 members known
(16598) 1992 YC2	50-250 k.y.	NV06	only 3 members known
(21509) Lucascavin	300-800 k.y.	NV06	only 3 members known
(300163) P/2006 VW139	7.5 ± 0.3 m.y.	No12b	main belt comet
P/2012 F5 (Gibbs)	1.5 ± 0.1 m.y.	No14	main belt comet

References: Ne0X = Nesvorný et al. (200X), NoXX = Novaković et al. (20XX), VNXX = Vokrouhlický and Nesvorný (20XX), VXX = Vokrouhlický et al. (20XX), NB04 = Nesvorný and Bottke (2004), T07 = Tsiganis et al. (2007), F06 = Farley et al. (2006), W08 = Willman et al. (2008), NV06 = Nesvorný and Vokrouhlický (2006), MH09 = Molnar and Haegert (2009).

bits ($t_{\text{age}} = 6.9 \pm 2.3$ m.y.).

There is a close relationship of the young asteroid families to the *asteroid dust bands* (see chapter by Jenniskens in this volume), which are strips of infrared emission running roughly parallel to the plane of the solar system (Low et al., 1984). The three most prominent dust bands, known as α , β and γ , have previously been thought to originate in the Themis, Koronis and Eos families (Dermott et al., 1984). A detailed modeling, however, have shown that the sources of these dust bands are the recently-formed Karin, Beagle and Veritas families (Dermott et al., 2002; Nesvorný et al., 2003, 2006, 2008b), mainly because: (1) the Veritas family with $i_P = 9.3^\circ$ provides a better fit to the latitudinal position of the γ band than the Eos family with $i_P \simeq 10^\circ$, and (2) the young families should now be more prolific sources of dust than the old families, because the dust production in a collisional cascade is expected to drop with time. A tracer of the Veritas family breakup has been found in measurements of extraterrestrial ^3He in $\simeq 8.2$ -m.y.-old deep ocean sediments (Farley et al., 2006).

4. V-SHAPE CRITERION

A correct identification of the brightest/largest members in a family is important for several reasons. For example, the spectroscopic observations are magnitude limited and can typically only be conducted for bright targets. The interpretation of spectroscopic observations of asteroid families, and implications for the homogeneity/heterogeneity of their parent bodies, therefore depend on whether the bright asteroids are the *actual* members of a family, or not (e.g., Reddy et al., 2011). The large objects in families are also critically important for asteroid impact studies, in which

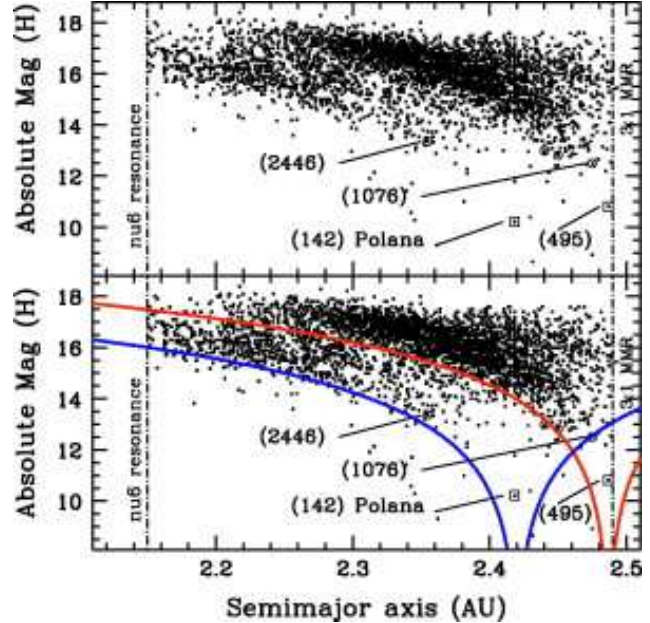


Fig. 5.— A recent application of the V-shape criterion to define the Polana and Eulalia families, and identify the largest members in these families (Walsh et al., 2013). The plot shows the absolute magnitude H of dark ($p_V < 0.1$) asteroids with $0.1 < e_P < 0.2$ and $i_P < 10^\circ$ as a function of a_P . The bottom panel illustrates the best-fit V-shape curves to the Polana (left) and Eulalia (right) families. (142) Polana and (495) Eulalia, the largest dark asteroids inside the left and right zones, respectively, are the likely largest members of the two families.

the Size Frequency Distribution (SFD) of family members is used to calibrate the results of impact experiments. Finally, the uncertainty in the membership of the largest fam-

ily members critically affects our estimates of size of the disrupted parent bodies (e.g., Durda et al., 2007).

While the interloper problem may not have an ideal solution, there exists a straightforward method that can be used to remove obvious bright/large interlopers based on dynamical considerations. This method is inspired by the “V-shape” of asteroid families, which becomes apparent when the absolute magnitude H of family members is plotted against a_P (Figure 5). The V shape results from two processes. First, larger (smaller) fragments tend to be ejected at lower (higher) speeds, and thus tend to be located, on average, closer to (further away from) the family center (see chapter by Michel et al. in this volume). The second and typically more dominant ‘V’ is contributed by the Yarkovsky effect.

The Yarkovsky effect (YE) is a recoil force produced by anisotropic emission of thermal photons from an asteroid surface (see chapter by Vokrouhlický et al. in this volume). The diurnal component of the YE, which is more important for asteroid-sized bodies than its seasonal counterpart, can increase the semimajor axis of an asteroid with a prograde rotation and decrease the semimajor axis for a retrograde rotation. The semimajor axis drift is generally given by $da_P/dt = \text{const.} \cos \theta / (a_P^2 D)$, where θ is the asteroid obliquity, D is the effective diameter, and the constant depends on material properties. The maximum drift occurs for $\theta = 0^\circ$ or $\theta = 180^\circ$. Thus, the envelope of the distribution of family members in (a_P, H) is expected to follow $|a_P - a_c| = C_{YE} 10^{H/5}$, where a_c is the family center (often assumed to coincide with the largest fragment), and C_{YE} is a constant related to t_{age} (Section 5). Interestingly, if the ejection speed $\delta V \propto 1/D$, as found for the youngest families (e.g., Nesvorný et al., 2006a) and some laboratory experiments (e.g., Fujiwara et al., 1989), then the ejection velocity field will produce the same dependence, $|a_P - a_c| = C_{EV} 10^{H/5}$, where C_{EV} is related to the magnitude of the ejection velocities.

These considerations allow us to define the V-shape criterion (e.g., Nesvorný et al., 2003). Consider a family extracted by the HCM as described in Section 2.2. Fit an envelope to the distribution of small family members in (a_P, H) using the functional dependence between a_P and H defined above. The envelope is then continued to low H values, and the bright members of the HCM family that fall *outside* the envelope boundaries can be rejected. On the other hand, the brightest HCM family members that fall *within* the envelope boundaries are good candidates for the largest family members. This method is illustrated in Figure 5.

In practice, a number of additional effects can complicate the application of the V-shape criterion described above. For example, strong nearby resonances can remove family members that drifted into them, thus producing cut-offs of the $a_P - a_c$ distribution beyond which no family members can be identified (e.g., the 3:1 resonance in Figure 5). Also, family members can be displaced in a_P by encounters with (1) Ceres and other massive main belt asteroids (Nesvorný et al., 2002b; Carruba et al., 2003, 2007a,

2012, 2013b; Delisle and Laskar, 2012). In addition, the physics of large scale collisions is still poorly understood, and the possibility that some large fragments can be accelerated to very high speeds cannot be ruled out. Therefore, while the V-shape criterion defined above is a useful guide, it cannot be *r rigidly applied*.

Possibly the best way to deal with this issue is to define the value of $C_0 = 10^{-H/5} |a_P - a_c|$ that best fits the V-shaped family envelope and report C_j/C_0 , where $C_j = 10^{-H_j/5} |a_{P,j} - a_c|$, for each family member j identified by the HCM. Asteroids with $|C_j/C_0| > 1$ can be flagged (but not removed), because they are potential interlopers in a dynamical family according to the V-shape criterion. The results can then be cross-linked with the spectroscopic data (or colors, or albedo measurements) to determine whether there is a good correspondence between the flagged bodies and (suspected) spectroscopic interlopers. An illustration of this procedure can be found in Vokrouhlický et al. (2006a) who examined the Eos family. They found that many large bodies in the HCM family with $|C_j/C_0| > 1$ have physical properties that are indeed incompatible (mainly dark C types) with the bulk of the Eos family (mainly brighter K types).

5. FAMILY AGE ESTIMATION

The method of backward integrations of orbits described in Section 3 cannot be used to determine ages of the families much older than ~ 10 m.y., mainly because the orbital evolution of main belt asteroids is generally unpredictable on long timescales and sensitively depends on non-gravitational effects that are difficult to model with the needed precision. Instead, the age of an old family can be estimated by a *statistical* method, which is based on the general notion that the spread of an asteroid family in a_P increases over time as its members drift away due to the Yarkovsky effect. Expressed in terms of the equations discussed in the previous section, the age can be estimated as

$$t_{\text{age}} \simeq 1 \text{ g.y.} \times \left(\frac{C_0}{10^{-4} \text{ AU}} \right) \left(\frac{a}{2.5 \text{ AU}} \right)^2 \times \left(\frac{\rho}{2.5 \text{ g cm}^{-3}} \right) \left(\frac{0.2}{p_V} \right)^{\frac{1}{2}} \quad (1)$$

where ρ is the asteroid bulk density and p_V is the visual albedo. While the equation above is scaled to typical values expected for an S-type asteroid, a change to $\rho = 1.5 \text{ g cm}^{-3}$ and $p_V = 0.05$, which would be more appropriate for a dark C-type asteroid, produces two multiplication factors that nearly compensate each other. The biggest uncertainty in the inversion from C_0 to t_{age} lies in the unknown density factor. Additional uncertainty, not explicitly apparent from Eq. (2), stems from the dependence of the drift rate on surface conductivity K . Together, the conversion from C_0 to t_{age} has an uncertainty of about a factor of 2.

More fundamentally, Eq. (1) neglects complicating factors such as the contribution of the original ejection field

and nearby resonances that can remove drifting bodies. If $C = C_{YE} + C_{EV}$, under the assumptions on the ejection speeds discussed in Section 4, the two effects cannot be decoupled from each other, and t_{age} estimated from C_0 will always overshoot the real age of the family. This happens, in essence, because this simple method only fits the family envelope.

Vokrouhlický et al. (2006a,b) have developed a more general statistical method that uses the actual distribution of family members within the V-shape envelope. It works as follows. First, the code generates a new-born family. The distribution of the ejection speeds of fragments is approximated by the Gaussian distribution in each velocity component with the size-dependent standard deviation $\delta V = V_5(5 \text{ km}/D)$, where V_5 is a free parameter. This functional dependence generally provides a good match to the ejection speeds inferred from the young families and impact simulations (Michel et al., 2001, 2003, 2004; Nesvorný et al., 2002a, 2006a; Durda et al., 2004, 2007). The Yarkovsky-YORP (hereafter YY) code then evolves the orbits of fragments accounting for the semimajor axis drift due to the YE, and the spin evolution from the YORP effect (Rubincam, 2000). To speed up the calculation, planetary perturbations were not taken into account in the original YY code (but see Masiero et al., 2012; results based on full N -body integrations are discussed in the following section).

When applied to an asteroid family, the goal is to find a combination of parameters V_5 and t_{age} that best fits the observed (a_P, H) distribution in the family. Since the model does not contain an SFD-related evolution component, this can be conveniently done by simply fitting the observed distribution of C_j . The results are found to be credible in cases such as the Erigone family (Figure 6), where the YY model is capable of adequately representing the observed C distribution, which shows void space near $C = 0$, a maximum at intermediate values of C , and a relatively sharp drop toward the largest C values seen in the family. This dependence is produced by the YORP effect which tilts the spin axis away from the orbital plane and therefore, through the $\cos \theta$ dependence of the YE, tends to maximize the drift rates. This gives some asteroid families the characteristic appearance in (a_P, H) , which different authors, with noticeably different gifts for subtleties of poetic expression, called “ears”, “wings” or “petals”.

But not all families have ears, wings or petals. In fact, most families have more uniform distribution of C that goes all the way from 0 to C_{max} . This is thought to have something to do with how the YE and YORP operate on g.y.-long timescales. It is perhaps related to the variability of the spin-related YORP torque, which sensitively depends on small perturbations of the asteroid surface. As a result of this dependence, the spin rate of each individual asteroid can undergo a random walk (stochastic YORP; Bottke et al., 2015) and, when spun down completely, the asteroid spin axis would chaotically tumble for some time, and subsequently reorient. This process could mix up the total drifts suffered by family members and, rather unpoetically,

remove the ears, wings or petals from the old families.

The application of the standard YY code (and, for that matter, also of the simple method based on the ‘V’-shape envelope) is problematic in cases when a family is cut by nearby mean motion resonances and looks like a box in (a_P, H) , or when C_{EV} is expected to be larger than C_{YE} , perhaps because the family’s parent was an object with large escape speed (e.g., the Vesta family; (4) Vesta has $V_{esc} \simeq 360 \text{ m s}^{-1}$), or because the family formed recently (e.g., the Datura, Karin, Veritas families have $C_{YE} \simeq 0$). A complete list of families to which the YY code was successfully applied so far is:

- Agnia ($t_{age} = 100 \pm 100 \text{ m.y.}$, $V_5 \simeq 15 \text{ m s}^{-1}$)
- Massalia ($t_{age} = 150 \pm 50 \text{ m.y.}$, $V_5 \simeq 20 \text{ m s}^{-1}$)
- Baptista ($t_{age} = 160 \pm 50 \text{ m.y.}$, $V_5 \simeq 40 \text{ m s}^{-1}$)
- Merxia ($t_{age} = 250 \pm 100 \text{ m.y.}$, $V_5 \simeq 25 \text{ m s}^{-1}$)
- Astrid ($t_{age} = 250 \pm 100 \text{ m.y.}$, $V_5 \simeq 15 \text{ m s}^{-1}$)
- Erigone ($t_{age} = 300 \pm 100 \text{ m.y.}$, $V_5 \simeq 30 \text{ m s}^{-1}$)
- Eos ($t_{age} = 1.3 \pm 0.5 \text{ g.y.}$, $V_5 \simeq 70 \text{ m s}^{-1}$)
- Tina ($t_{age} = 170 \pm 50 \text{ g.y.}$, $V_5 \simeq 20 \text{ m s}^{-1}$) .

Here we have taken the liberty to update and round off the estimates, and give more generous errors than in the original publications (Vokrouhlický et al., 2006a,b,c; Bottke et al., 2007; Carruba and Morbidelli, 2011; see also Carruba, 2009a for the Padua family). Note that these errors do not include the uncertainty of about a factor of 2 from the poorly known bulk density and surface conductivity of the asteroids in question. Including this uncertainty, Masiero et al. (2012) found that the best-fitting age of the Baptista family can be anywhere between 140 and 320 m.y.

The estimated ejection speeds are $V_5 = 15\text{--}50 \text{ m s}^{-1}$, except for the Eos family, which formed in a breakup of a very large parent asteroid ($D_{PB} \sim 300 \text{ km}$). These results are consistent with the ejection speeds inferred from the young Karin family, which has $V_5 \simeq 15 \text{ m s}^{-1}$ for a relatively small parent body ($D_{PB} \simeq 35 \text{ km}$; Nesvorný et al., 2006a). The ejection speeds contribute by $\simeq 20\%$ (for oldest Eos) to 50% (for youngest Agnia) to the total family spread in the semimajor axis. Ignoring this contribution, as in Eq. (2), would thus lead to an overestimate of t_{age} by $\simeq 20\text{--}50\%$. While one must therefore be careful in applying Eq. (2) to the small/young families that did not have enough time to significantly spread by the YE, the effect of the ejection speeds should be less of an issue for old families.

6. DYNAMICAL EVOLUTION

6.1 INITIAL STATE

The dynamical evolution of asteroids in families is similar to the dynamical evolution of main belt asteroids in

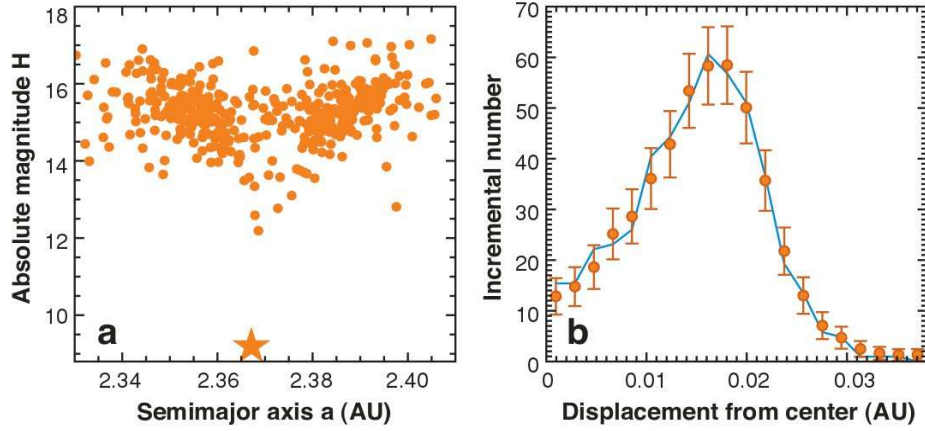


Fig. 6.— (a) The Ergone family projected onto a plane of proper semimajor axis versus absolute magnitude H ; (163) Ergone is the filled star. The family has been separated into two clouds ($a_p \lesssim 2.37$ AU; $a_p \gtrsim 2.37$ AU) by the Yarkovsky/YORP evolution. (b) A comparison between model results (solid line) and binned Ergone family (gray dots; see Vokrouhlický et al., 2006b). The error bars are the square root of the number of bodies in each bin. The x -axis is the distance of family members from the the family center. Based on this result, Vokrouhlický et al. (2006b) estimated that $t_{\text{age}} = 280^{+30}_{-50}$ m.y. and $V_5 = 26^{+14}_{-11}$ m s $^{-1}$, where the error bars do *not* include the uncertainty originating from uncertain material properties (e.g., density, surface conductivity).

general. Studying the dynamical evolution of individual families is useful in this context, because we more or less know how the families should look like initially. Things may thus be learned by comparing these ideal initial states with how different families look now, after having dynamically evolved since their formation. The dynamical studies can also often provide an independent estimate of t_{age} .

Assuming that $\delta V \ll V_{\text{orb}}$, the initial shape of families in (a, e, i) can be obtained from the Gauss equations (e.g., Zappalà et al., 2002), which map the initial velocity perturbation $\delta \mathbf{V} = (V_R, V_T, V_Z)$, where V_R , V_T and V_Z are the radial, tangential and vertical components of the velocity vector, to the change of orbital elements $\delta \mathbf{E} = (\delta a, \delta e, \delta i)$. If the ejection velocity field is (roughly) isotropic, the Gauss equations imply that initial families should (roughly) be ellipsoids in (a, e, i) centered at the reference orbit (a^*, e^*, i^*) . The transformation from (a, e, i) to (a_P, e_P, i_P) preserves the shape, but maps (a^*, e^*, i^*) onto (a_P^*, e_P^*, i_P^*) such that, in general, $a_P^* \neq a^*$, $e_P^* \neq e^*$ and $i_P^* \neq i^*$.

The shape of the ellipsoids in (a_P, e_P, i_P) is controlled by the true anomaly f and the argument of perihelion ω of the parent body at the time of the family-forming breakup. The projected distribution onto the (a_P, e_P) plane is a tilted ellipse with tightly correlated a_P and e_P if the breakup happened near perihelion (see Figure 3a) or tightly anticorrelated a_P and e_P if the breakup happened near aphelion. The two recently-formed families for which this shape is clearly discernible, the Karin and Veritas families, have correlated a_P and e_P , implying that $|f| \simeq 30^\circ$ (Figures 3 and 4).

The projected initial distribution onto the (a_P, i_P) plane is an ellipse with horizontal long axis and vertical short axis. The short-to-long axis ratio is roughly given by $\cos(\omega + f)V_Z/V_T$. Thus, breakups near the ascending

$(\omega + f \simeq 0)$ and descending $(\omega + f \simeq \pi)$ nodes should produce ‘fat’ ellipses while those with $\omega + f = \pm\pi/2$ should make ‘squashed’ ellipses with $\delta i_P \simeq 0$. While the Karin family neatly fits in this framework with $\omega + f \simeq \pi/4$ (Figure 3), the Veritas family shows large δi_P values, indicating that the ejection velocity field should have been anisotropic with V_Z some $\simeq 2$ -4 times larger than V_T .

The reference orbit (a_P^*, e_P^*, i_P^*) is often taken to coincide with the proper orbit of a largest family member. This should be fine for families produced in cratering or mildly catastrophic events, where the orbital elements of the impacted body presumably did not change much by the impact. For the catastrophic and highly catastrophic breakups, however, the largest surviving remnant is relatively small and can be significantly displaced from the family’s center. For example, (832) Karin, the largest $\simeq 17$ -km-diameter member of the Karin family produced by a catastrophic breakup of a $\simeq 40$ -km-diameter parent body (mass ratio ~ 0.08 ; Nesvorný et al., 2006a), is displaced by -0.002 AU from the family center ($\simeq 20\%$ of the whole extension of the Karin family in a_P). This shows that, in general, the position of the largest fragment does not need to perfectly coincide with the family center, and has implication for the V-shape criterion discussed in Section 4 (where an allowance needs to be given for a possible displacement).

6.2 DYNAMICS ON GIGAYEAR TIMESCALES

An overwhelming majority of the observed asteroid families are not simple Gaussian ellipsoids. While this was not fully appreciated at the time of the Asteroids III book, today’s perspective on this issue is clear: *the families were stretched in a_P as their members drifted away from their original orbits by the Yarkovsky effect.* The asteroid families found in the present main belt are therefore nearly hor-

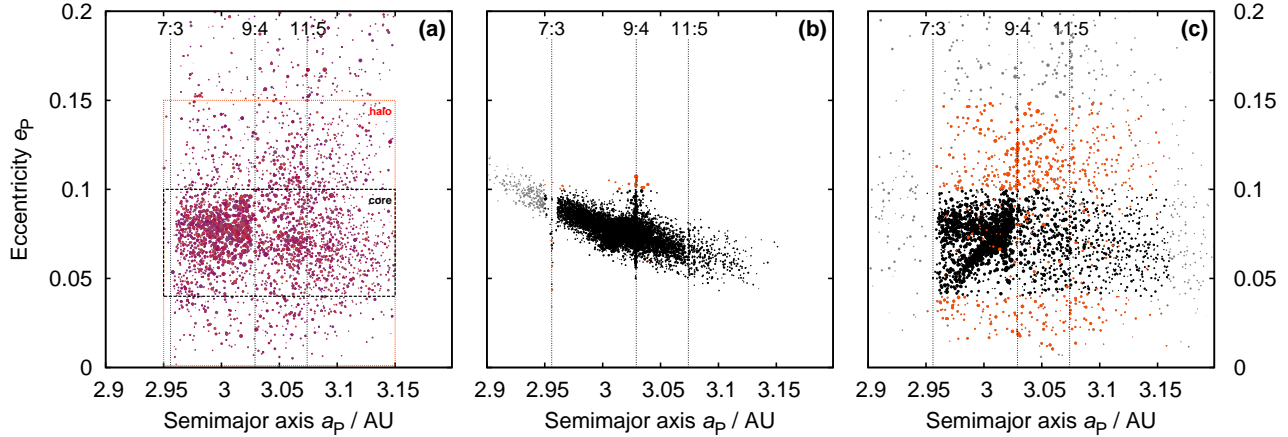


Fig. 7.— Dynamical evolution of the Eos family. From left to right, the panels show the: (a) observed family and its halo in the (a_P, e_P) projection, (b) assumed initial shape of the family, and (c) family's structure after 1.7 g.y. In (a), we plot all asteroids with Eos-family colors ($0.0 < a^* < 0.1$ mag and $-0.03 < i - z < 0.08$ mag; see Ivezić et al. (2001) for the definition of color indices from the SDSS). The size of a symbol is inversely proportional to absolute magnitude H . The boxes approximately delimit the extent of the core and halo of the Eos family. In (b), 6545 test particles were distributed with assumed isotropic ejection velocities, $V_5 = 93 \text{ m s}^{-1}$, $f = 150^\circ$ and $\omega = 30^\circ$. Nearly all initial particles fall within the family core. In (c), an N -body integrator was used to dynamically evolve the orbits of the test particles over 1.7 g.y. The integration included gravitational perturbations from planets, and the Yarkovsky and YORP effects. The vertical lines show the locations of several resonances that contributed to spreading of orbits in e_P (7:3, 9:4 and 11:5 with Jupiter, also 3J-2S-1 and $z_1 \equiv g + s - g_6 - s_6 = 0$). Adapted from Brož and Morbidelli (2013).

izontal and elongated structures in (a_P, e_P) and (a_P, i_P) . This shows that the original ejection velocity field *cannot* be easily reconstructed by simply mapping back today's (a_P, e_P, i_P) to (V_R, V_T, V_Z) from the Gauss equations (Note 7).

Moreover, many asteroid families have weird shapes which, taken at the face value, would imply funny and clearly implausible ejection velocity fields. A prime example of this, briefly mentioned in section 2.2, is the Koronis family (Bottke et al., 2001). Since the case of the Koronis family was covered in the Asteroids III book (chapter by Bottke et al., 2002), we do not discuss it here. Instead, we concentrate on the results of new dynamical studies, many of which have been inspired by the Koronis family case. The dynamical effects found in these studies fall into three broad categories:

(1) Members drifting in a_P encounter a mean motion resonance with one of the planets (mainly Jupiter, Mars or Earth; see chapter Nesvorný et al., 2002c in Asteroids III book). If the resonance is strong enough (e.g., 3:1, 2:1, or 5:2 with Jupiter), the orbit will chaotically wander near the resonance border, its eccentricity will subsequently increase, and the body will be removed from the main belt and transferred onto a planet-crossing orbit (Wisdom, 1982). If the resonance is weak, or if the asteroid is small and drifts fast in a_P , the orbit can cross the resonance, perhaps suffering a discontinuity in e_P during the crossing, and will continue drifting on the other side. If the resonance is weak and the drift rate is not too large, the orbit can be captured in the resonance and will slowly diffuse to larger or smaller eccentricities. It may later be released from the resonance with e_P that can be substantially different from the origi-

nal value. The effects of mean motion resonances on i_P are generally smaller, because the eccentricity terms tend to be more important in the resonant potential. The inclination terms are important for orbits with $i_P \gtrsim 10^\circ$. A good example of this is the Pallas family with $i_P \simeq 33^\circ$ (Carruba et al., 2011).

(2) Drifting members meet a secular resonance. The secular resonances are located along curved manifolds in (a_P, e_P, i_P) space (Knežević et al., 1991). Depending on the type and local curvature of the secular resonance, and asteroid's da/dt , the orbit can be trapped inside the resonance and start sliding along it, or it can cross the resonance with a noticeably large change of e_P and/or i_P . A good example of the former case are orbits in the Eos family sliding along the $z_1 = g - g_6 + s - s_6 = 0$ resonance (Vokrouhlický et al., 2006a). An example of the latter case is the Koronis family, where eccentricities change as a result of crossing of the $g + 2g_5 - 3g_6 = 0$ resonance (Bottke et al., 2001). If the secular resonance in question only includes the g (or s) frequency, effects on e_P (or i_P) are expected. If the resonance includes both the g and s frequencies, both e_P and i_P can be effected. If the orbit is captured in a resonance with the g and s frequencies, it will slide along the local gradient of the resonant manifold with changes of e_P and i_P depending on the local geometry.

(3) Encounters with (1) Ceres and other massive asteroids produce additional changes of a_P , e_P and i_P (Nesvorný et al., 2002b; Carruba et al., 2003, 2007a, 2012, 2013b; Delisle and Laskar, 2012). These changes are typically smaller than those from the Yarkovsky effect on a_P and resonances on e_P and i_P . They are, however, not negligible. The effect of encounters can be approximated by a random

walk (see Carruba et al., 2007a for a discussion). The mean changes of a_P , e_P and i_P increase with time roughly as \sqrt{t} . The asteroid families become puffed out as a result of encounters, and faster so initially than at later times, because of the nature of the random walk. Also, a small fraction of family members, in some cases perhaps including the largest remnant, can have their orbits substantially affected by a rare, very close encounter. Additional perturbations of asteroid orbits arise from the linear momentum transfer during non-disruptive collisions (Dell’Oro and Cellino, 2007).

6.3 DISCUSSION OF DYNAMICAL STUDIES

The Koronis family case (Bottke et al., 2001) sparked much interest in studies of the dynamical evolution of asteroid families on very long timescales. Here we review several of these studies roughly in the chronological order. The goal of this text is to illustrate the dynamical processes discussed in the previous section on specific cases.

Nesvorný et al. (2002b) considered the dynamical evolution of the Flora family. The Flora family is located near the inner border of the main belt, where numerous mean motion resonances with Mars and Earth produce slow diffusion of e_P and i_P . The numerical integration of orbits showed how the overall extent of the Flora family in e_P and i_P increases with time. The present width of the Flora family in e_P and i_P was obtained in this study after $t \simeq 0.5$ g.y. even if the initial distribution of fragments in e_P and i_P was very tight. The Flora family expansion saturates for $t > 0.5$ g.y., because the Flora family members that diffused to large eccentricities are removed from the main belt by encounters with Mars (the Flora family is an important source of chondritic near-Earth asteroids (NEAs); Vernazza et al., 2008). The present spread of the Flora family in a_P , mainly contributed by the Yarkovsky effect, indicates $t_{\text{age}} \sim 1$ g.y.

Carruba et al. (2005) studied the dynamical evolution of the Vesta family. The main motivation for this study was the fact that several inner main belt asteroids, such as (956) Elisa and (809) Lundia, have been classified as V-types from previous spectroscopic observations (Florczak et al., 2002), indicating that they may be pieces of the basaltic crust of (4) Vesta. These asteroids, however, have orbits rather distant from that of (4) Vesta and are not members of the Vesta’s dynamical family even if a very large cutoff distance is used. It was therefore presumed that they: (i) have dynamically evolved to their current orbits from the Vesta family, or (ii) are pieces of differentiated asteroids unrelated to (4) Vesta. Carruba et al. (2005) found that the interplay of the Yarkovsky drift and the $z_2 \equiv 2(g - g_6) + s - s_6 = 0$ resonance produces complex dynamical behavior that can, indeed, explain the orbits of (956) Elisa and (809) Lundia, assuming that the Vesta family is at least $\simeq 1$ g.y. old. This gives support to (i).

In a follow-up study, Nesvorný et al. (2008a) performed a numerical integration of 6,600 Vesta fragments over 2 g.y. They found that most V-type asteroids in the inner main belt can be explained by being ejected from (4) Vesta and dy-

namically evolving to their current orbits outside the Vesta family. These V-type “fugitives” have been used to constrain the age of the Vesta family, consistently with findings of Carruba et al. (2005), to $t_{\text{age}} \gtrsim 1$ g.y. Since previous collisional modeling of the Vesta family suggested $t_{\text{age}} \lesssim 1$ g.y. (Marzari et al., 1999), the most likely age of the Vesta family that can be inferred from these studies is $t_{\text{age}} \sim 1$ g.y. This agrees well with the age of the $\simeq 500$ -km-diameter Rheasilvia basin on (4) Vesta inferred from crater counts ($\simeq 1$ g.y.; Marchi et al., 2012) (Note 8).

Vokrouhlický et al. (2006a) studied the dynamical evolution of the Eos family. The Eos family has a complicated structure in proper element space leading some authors to divide it in several distinct families (e.g., Milani et al., 2014). Diagnostically, however, the Eos family, although somewhat physically heterogeneous, has the color, albedo and spectral properties that contrast with the local, predominantly C-type background in the outer asteroid belt. This suggests that this is a single family. As we discuss below, the complicated structure of the Eos family arises from the presence of several mean motion and secular resonances.

To start with, Vokrouhlický et al. (2006a) showed that the Eos family members drifting by the Yarkovsky effect into the 7:3 resonance with Jupiter are removed (see Figure 7). This cuts the family at 2.957 AU. Members drifting with $da/dt > 0$, on the other hand, will encounter the 9:4 resonance at 3.03 AU. This resonance, being of higher order and thus weaker, is not an unpenetrable barrier, especially for smaller members with higher drift rates. The estimated fraction of bodies that can cross the 9:4 resonance is $< 10\%$ for $H < 12$ but reaches $\simeq 35\%$ for $H = 16$. This is consistent with the magnitude distributions of the Eos family members on both sides of the 9:4 resonance. The larger dispersion of the part of the Eos family with $a_P > 3.03$ AU is contributed by perturbations of e_P and i_P during the 9:4 resonance crossing (Figure 7). Finally, many orbits in the central part of the Eos family are trapped in the secular resonance $z_1 \equiv g + s - g_6 - s_6 = 0$, and slide along it while drifting in a_P (Note 9).

Finally, we discuss additional processes whose significance is shadowed by the Yarkovsky effect and resonances, but which can be important in some cases. Nesvorný et al. (2002b) considered encounters with (1) Ceres and found that the characteristic change of the semimajor axis due to these encounters is $\Delta a \simeq 0.001$ AU over 100 m.y. Assuming that the scattering effect of encounters can be described by a random walk with $\Delta a \propto \sqrt{t}$, the expected changes over 1 g.y. and 4 g.y. are $\simeq 0.003$ AU and $\simeq 0.007$ AU, respectively. The orbital changes were found to be larger for orbits similar to that of (1) Ceres, because the orbital proximity leads to lower encounter speeds, and larger gravitational perturbations during the low-speed encounters. Carruba et al. (2003) studied the effect of encounters on the Adeona and Gefion families, both located near (1) Ceres in proper element space. They found that the semimajor axis of members of the Adeona and Gefion families can change

by up to ~ 0.01 AU over the estimated age of these families.

With similar motivation, Carruba et al. (2007a) considered the effect of encounters of the Vesta family members with (4) Vesta. They found the characteristic changes $\Delta a = 0.002$ AU, $\Delta e = 0.002$ and $\Delta i = 0.06^\circ$ over 100 m.y. In a follow-up work, Delisle and Laskar (2012) included the effects of eleven largest asteroids. They showed that encounters of the Vesta family members with (4) Vesta and (1) Ceres are dominant, contributing roughly by 64% and 36% to the total changes, respectively. The functional dependence $\Delta a = 1.6 \times 10^{-4} \sqrt{t/1}$ m.y. AU was used in this work to extrapolate the results to longer time intervals. Moreover, Carruba et al. (2013b) studied the influence of these effects on the Pallas, Hygiea and Euphrosyne families. They showed that the effects of (2) Pallas –the 3rd most massive main-belt asteroid– on the Pallas family are very small, because these asteroids have high orbital inclinations ($i_P \simeq 33^\circ$), lower frequency of encounters and higher-than-average encounter speeds.

Dell’Oro and Cellino (2007) pointed out that orbits of main belt asteroids can change as a result of the linear momentum transfer during non-destructive collisions. They found that the expected semimajor axis change from these collisions for a $D = 50$ -km main-belt asteroid is $\Delta a \sim 10^{-4}$ AU over 100 m.y. (with the scaling laws from Benz and Asphaug, 1999). This is an order of magnitude lower than the change expected from close encounters with large asteroids and comparable to the sluggish drift rate expected from the Yarkovsky effect for $D = 50$ km. For $D < 50$ km, the orbital changes from non-destructive collisions sensitively depend on several unknown parameters, such as the SFD of sub-km main-belt asteroids, but the general trend is such that Δa drops with decreasing D (assuming that the cumulative SFD index is < 4 ; Dell’Oro and Cellino, 2007). Since Δa is independent of D for encounters with (1) Ceres, and $\Delta a \propto 1/D$ for the Yarkovsky force, these two effects outrun the non-destructive collisions for $D < 50$ km. This limits the significance of non-destructive collisions for the dynamical evolution of asteroid families. Their effect on e_P and i_P is also minor.

6.4 FAMILY HALOS

When dynamical families are identified and removed from the main belt, they leave behind holes in the distribution of proper elements that are surrounded by regions with increased asteroid density (Figure 8). These peripheral regions are known as the family *halos*. The families and family halos surrounding them are clearly related, which can most conveniently be demonstrated by considering their physical properties. For example, the Koronis family and its halo consist of bright asteroids (mean albedo $p_V = 0.15$) that are classified as S in the asteroid taxonomy (moderate spectral slope and shallow absorption band near $1 \mu\text{m}$). These properties contrast with the local background in the outer main belt, which is mostly dark ($p_V \simeq 0.05$) and C-type (featureless neutral spectrum). The Eos family and its

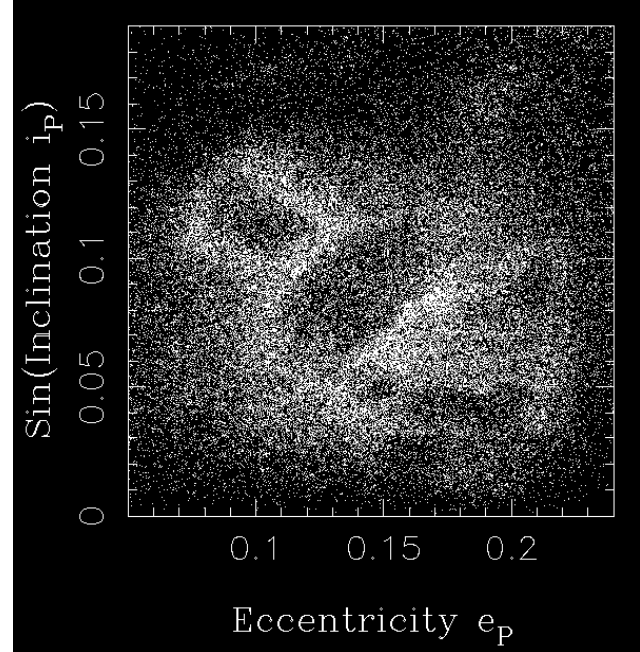


Fig. 8.— The halos of families in the inner main belt ($2 < a_P < 2.5$ AU). The dynamical families were identified by the HCM in 3D of proper elements and were removed, leaving behind what resembles a fuzzy chalk contour of victim’s body removed from a crime scene. The head, body and bottom leg correspond to the locations of the Vesta, Flora and Nysa-Polana families. The halos surrounding these families, mainly composed of small asteroids, are rather dramatic in this projection. This figure illustrates a major weakness of the traditional family-identification method based on the HCM in 3D space of proper elements.

halo (K-type, $p_V = 0.13$) also stand out from the dark outer belt background.

The distinction between families and family halos is, in a sense, formal, because it appears as a consequence of the identification method. Indeed, to extract the family halo by applying the HCM in 3D space of proper elements, one would need to increase the value of the d_{cut} parameter. If it is increased, however, the identification would fail due to the problem of chaining (Section 2.2). This is a consequence of the fact that the number density of halo asteroids is comparable to, or only slightly larger than, the number density of background asteroids. A better method for extracting the families jointly with their halos consists in applying the HCM in space of extended dimensions, where physical properties are used in addition to the proper elements (Section 2.5; Parker et al., 2008; Carruba et al., 2013a; Masiero et al., 2013).

The origin of family halos is contributed by at least two processes. In the case of the Eos family, the observed dispersion of halo in e_P and i_P is too large (0-0.15 and $7-14^\circ$, respectively) to be related to the the ejection speeds. Instead, Brož and Morbidelli (2013) showed how the Eos family halo gradually appears as a result of complex orbital dynamics in the Eos family region (Figure 7). The age of

the Eos family inferred from that work, $1.5 \text{ g.y.} < t_{\text{age}} < 2.2 \text{ g.y.}$, is larger than the one obtained from the YY code ($t_{\text{age}} = 1.3 \pm 0.2 \text{ g.y.}$; Vokrouhlický et al., 2006a and Section 5), but the two estimates are consistent at the 1σ level.

The Koronis family and its halo, on the other hand, are located in a dynamically quiet region of the main belt ($2.82 < a_P < 2.95 \text{ AU}$, $e_P \simeq 0.045$, $i_P \simeq 2^\circ$) where no major resonances exist (except for $g + 2g_5 - 3g_6 = 0$; Bottke et al., 2001). The long-term dynamics of the Koronis family therefore has a relatively small influence on the overall width of the family in e_P and i_P . In contrast, the present shift of the Koronis family/halo members from the family's center is relatively large (up to $\simeq 0.015$ in e_P and 0.5° in i_P). This can plausibly be explained by the ejection speeds.

Assuming an isotropic ejection velocity field and $\delta V = V_5(5 \text{ km}/D)$ with $V_5 = 50 \text{ m s}^{-1}$, we find that $\delta a_P/a_P \simeq 2\delta V/V_{\text{orb}} \simeq 0.018$ for $D = 5 \text{ km}$ fragments. This represents a small share of the Koronis family width in a_P (the population of $D = 5 \text{ km}$ members stretches from the 5:2 resonance at 2.82 AU to the 7:3 resonance at 2.95 AU), consistently with the idea that the observed spread in a_P is mainly due to the Yarkovsky effect. With $D = 1.5 \text{ km}$, which is roughly the size of the smallest asteroids observed in this part of the main belt, the expected changes are $\delta e_P = (1\text{-}2) \times \delta V/V_{\text{orb}} \simeq 0.015$ and $\delta i_P \lesssim \delta V/V_{\text{orb}} \simeq 0.6^\circ$. This is comparable to the present width of the Koronis family/halo in e_P and i_P .

Another notable argument in this context is that the Koronis halo is populated by small asteroids with diameters near the minimum detectable size (while the big ones are inside the family core). This suggests a certain size dependency of the process that created the halo, presumably related to the size dependency of the ejection speeds (see chapter by Michel et al. in this volume). This important trend was pointed out by Cellino et al. (2004), and was further discussed in Cellino et al. (2009).

7. SYNTHESIS

7.1 METHOD, FAMILY NAMES AND FIN

Here we present a synthesis of asteroid families extracted from many past publications (Mothé-Diniz et al., 2005; Nesvorný et al., 2005; Gil-Hutton, 2006; Parker et al., 2008; Nesvorný 2010, 2012; Novaković et al., 2011; Brož et al., 2013; Masiero et al., 2011, 2013; Carruba et al., 2013a; Milani et al., 2014). The synthesis is based on the numerically computed proper elements (AstDyS catalog from August 2014 with the proper elements for 384,337 numbered asteroids; the proper elements of 4016 Jupiter Trojans were taken from Rozehnal and Brož 2013) and the latest releases of data from the SDSS and WISE.

First, we collected a long list of all (they were 228) families reported in these publications. Second, we checked to see whether the clustering in proper elements of each reported group is meaningful, and whether the group has re-

asonably homogeneous colors and albedos (see methods in Section 2). The families that passed the preliminary tests were scrutinized further to establish the best cutoff value d_{cut} (the values of d_{cut} were informed from past publications), apply the V-shape criterion to identify large interlopers (section 4), and estimate t_{age} from the envelope-based method (Section 5).

We made sure that each identified group with d_{cut} was complete (i.e., not missing any extension that would make sense dynamically), and not part of a larger structure. In some cases, a cut in proper element space was applied to avoid the problem of chaining. In several cases, following Masiero et al. (2013), we used an albedo cutoff, $p_V < 0.15$, to identify dark families in the inner and central belts (the (84) Klio, (313) Chaldaea, (2262) Mitidika families). Finally, we removed all identified families and searched for significant groups in the leftover population. This led to the identification of several additional families (e.g., the (589) Croatia, (926) Imhilde, (1332) Marconia families in the outer belt).

A difficulty we had to deal with is that different authors often listed the same family under different names. For example, Masiero et al. (2013) renamed the families after their largest fragments (e.g., the (158) Koronis family was referred to as the (208) Lacrimosa family). While it is very useful to identify the largest fragment, this naming convention creates chaos because some well-established family names disappear (Koronis, Maria, Flora, Gefion, Dora, etc.) and new names are used to refer to the same groups (Lacrimosa, Roma, Augusta, Gudiachvili, Zhongolovich, etc.). It is also not clear in many cases what the true largest member is ((208) Lacrimosa is only slightly larger than (158) Koronis, some large objects have peripheral orbits and can be interlopers, etc.).

A simple solution to this problem is to think of the family names as of *labels*, used from historical and other reasons, which do not necessarily reveal what the largest or lowest-numbered asteroid is. Thus, the Koronis family would remain the Koronis family, regardless of whether (158) Koronis, (208) Lacrimosa or some other large asteroid are the actual family members, largest or not.

Anticipating that some authors will still prefer to rename some families, here we assign each family a unique Family Identifier Number (FIN). The FIN goes from 101 to 399 for families identified from the analytic proper elements: 1XX for the inner belt (2-2.5 AU), 2XX for the middle belt (2.5-2.82 AU), and 3XX for the outer belt (2.82-3.7 AU). The families identified from the synthetic proper elements were assigned the FIN from 401 to 999: 4XX and 7XX for the low and high inclination families in the inner belt, 5XX and 8XX for the low and high inclination families in the middle belt, and 6XX and 9XX for the low and high inclination families in the outer belt. The division between low and high inclinations was taken at $\sin i_P = 0.3$ ($i_P \simeq 17.5^\circ$) which coincides with the highest inclinations for which the analytic proper elements are available. The FINs of the low-inclination families are 'aligned' such that 101 and 401, 102

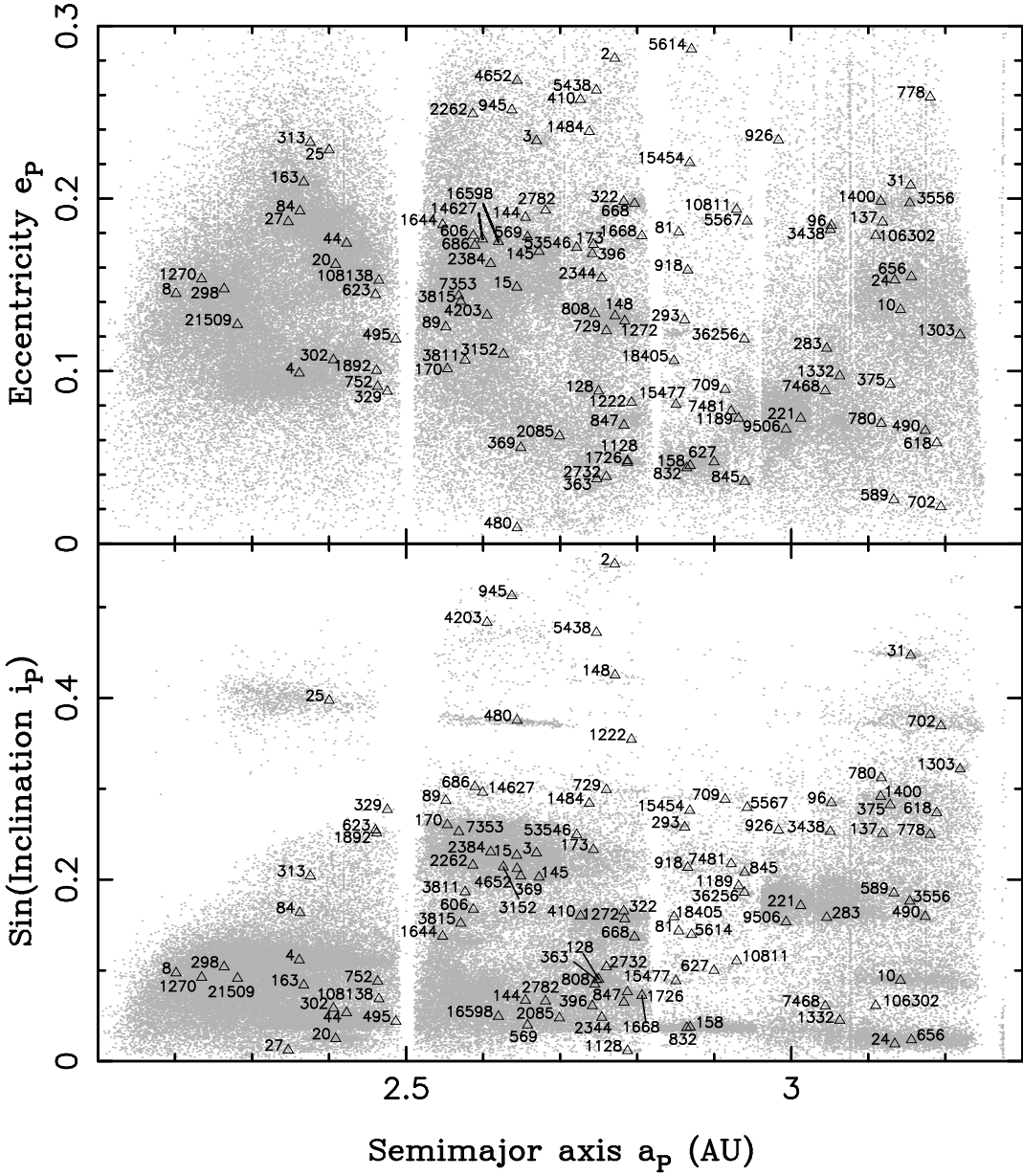


Fig. 9.— The orbital location of notable families from Table 2. A triangle is placed at the orbit of an asteroid after which the family is named. The label near the triangle shows the designation number of that asteroid.

and 402, 201 and 501, etc., are the same families identified from two different datasets. The families among Hungarias with $a < 2$ AU, Hildas with $a \simeq 3.8$ AU, and Jupiter Trojans with $a \simeq 5.2$ AU are given the FIN between 001 and 099.

The main idea behind this notation is that even if a family is eventually renamed, its FIN will remain the same. Therefore, it should suffice to list the FIN of the renamed family in a new publication to make it clear how the new name relates to the designation(s) used in the past. For example, the Koronis family is given the FIN equal to 605 (synthetic proper elements, outer belt, low i , 5th notable family), and will remain 605 even if the name Lacrimosa family will eventually be adopted. Since, however, it can

be easily checked that the Koronis and Lacrimosa families have the same FIN (assuming that authors list the FIN in their publications), it will be crystal clear that we deal the same family.

A potential difficulty with this scheme would arise if families that were previously assigned a FIN are often found to be nonexistent (say, because they are later found statistically insignificant or part of a large structure that was not evident in the original data). We suggest that such families are deleted and the associated FINs are left void (i.e., not assigned to any family) such that there is no source for confusion. Finally, to avoid having many void FINs and not to run out of the FINs with the three digit scheme described above, the FIN should be given only to families that are

reasonably secure. Other, less secure families can be tentatively listed as family candidates and can wait for their FIN until the situation becomes clear with the new data. If the number of families in the inner, middle and/or outer belts exceeds 99, the 3-digit FIN scheme described here can be easily modified to a 4-digit scheme by adding 0 at the second decimal digit, such that, e.g., FIN=401 (the Vesta family) becomes FIN=4001. This change can be implemented if the need arises.

7.2 FAMILY LISTS

There are 122 notable asteroid families reported in Table 2 and 19 family candidates in Note 11. The vast majority of families listed in Table 2 have been reported in many past publications and are clear beyond doubt (Vesta, Massalia, Eunomia, Gefion, Koronis, Eos, Themis, etc.). Many additional families, reported in only one or two previous publications, are also clear beyond doubt with the new data. Eleven families are reported here for the first time ((329) Svea and (108138) 2001 GB11 in the inner belt, (89) Julia, (369) Aeria, (1484) Postrema, (2782) Leonidas and (3152) Jones in the central belt, (589) Croatia, (926) Imhilde, (1332) Marconia and (106302) 2000 UJ87 in the outer belt). There are 20 notable families in the inner belt (the Nysa-Polana complex is counted as 3 families here), 47 in the central belt, 46 in the outer belt, 2 among Hildas in the 3:2 resonance with Jupiter, 1 in Hungarias, and 6 among Jupiter Trojans. Of these, seventeen have high orbital inclination ($i_P > 17.5^\circ$). Figure 9 shows the orbital location of the notable families in the main belt.

The lists of members of the notable families can be downloaded from the PDS node (Note 10). Each list contains the following information: (1) the asteroid number, (2) a_P , (3) e_P , (4) $\sin i_P$, and (5) the absolute magnitude H from the Minor Planet Center. Also, for families that have the V-shape envelope in (a_P, H) , we fit C_0 to this shape (Section 4, column 7 in Table 2) and report C_j/C_0 for each family member in column 6 of the PDS files. The average albedo of each family was obtained from the WISE, and is reported in column 9 of Table 2 (p_V). The taxonomic type of families, reported in column 8 of Table 2, was taken from the previous taxonomic classification of families (Cellino et al. 2002) or was deduced from the SDSS colors.

Columns 5 and 6 of Table 2 report the estimated diameter of the largest member, D_{LM} , and diameter of a sphere with volume equivalent to that of all fragments, D_{frag} . D_{LM} was obtained from AKARI, if available, or from WISE, if available, or was estimated from H and average p_V . The largest member and suspected interlopers with $|C_j/C_0| > 2$ were excluded in the estimate of D_{frag} . The comparison of D_{LM} and D_{frag} helps to establish whether a particular breakup event was catastrophic ($D_{frag} > D_{LM}$) or cratering ($D_{frag} < D_{LM}$), but note that this interpretation may depend on sometimes uncertain membership of the largest family objects. Also, the diameter of the parent body of each family can be estimated as $D_{PB} = (D_{LM}^3 + D_{frag}^3)^{1/3}$,

but note that this estimate ignores the contribution of small (unobserved) fragments.

7.3 COMPARISON WITH PREVIOUS DATASETS

The family synthesis presented here is consistent with the results reported in Nesvorný (2012), Brož et al. (2013) and Carruba et al. (2013a). For example, all families reported in Nesvorný (2012) were found to be real here (except the (46) Hestia family that was moved to candidates; see Note 11). Nesvorný (2012), however, used very conservative criteria for the statistical significance of a family, and reported only 76 families (or 78 if the Nysa-Polana complex is counted, as it should, as three families). Using the 2014 catalog of proper elements, albedo information from Masiero et al. (2013), and validating several new families from Milani et al. (2014), here we collect 44 families that did not appear in Nesvorný (2012). Almost all families reported in Brož et al. (2013) also appear here (a notable exception is a large group surrounding (1044) Teutonia, which we believe is not a real family; see Note 11), but many new cases were added. The correspondence with Carruba et al. (2013a) is also good.

Parker et al. (2008) used $N_{min} = 100$ and therefore missed many small families which did not have more than 100 members in the 2008 catalog. Also, given that they used a subset of asteroids with the SDSS colors, even relatively large families were unnoticed in this work (e.g. the (752) Sulamitis family in the inner belt now has 303 members). The high- i families were not reported in Parker et al. (2008), because they only used the analytic proper elements which are not available for the high- i orbits. The strength of Parker et al.'s identification scheme was the reliability. Indeed, of all families reported in Parker et al. (2008) only the (1044) Teutonia, (1296) Andree and (2007) McCuskey (part of the Nysa-Polana complex) are not included among the notable families here (Parker et al.'s (110) Lydia family appears here as the (363) Padua family).

Masiero et al. (2013; hereafter M13) reported 28 new cases and found that 24 old families were lost when compared to the family lists in Nesvorný (2012). Most families not listed in M13 are well-defined families such as Karin, Beagle, Datura, Emilkowalski, Lucascavin, etc. These families were not listed in M13, because they overlap with larger families (and were included in their membership lists in M13) or because they only have a few known members (i.e., fall below N_{min} used in M13). On the other hand, we verified that many new cases reported in Masiero et al. (2013) are genuine new families that can be conveniently found with the albedo cutoff (e.g., the (84) Klio, (144) Vibilia, (313) Chaldaea (= (1715) Sall in M13), (322) Phaeo, (623) Chimarea, (816) Juliana, and (1668) Hanna families). These families were included here. In some cases, we found that M13's new family barely stands out from the background and it thus seems uncertain. To stay on the safe side, we therefore report these cases as the candidate families in Note 11. These families may be real, but their statistical

significance needs to be carefully tested with the new data.

Finally, we compare the family synthesis with Milani et al. (2014; hereafter M14), who used the newest catalogs from all previous works discussed here. They identified many new families which are certain beyond doubt (e.g., the (96) Aegle, (618) Elfriede, (2344) Xizang, (3438) Inar-radas, (3811) Karma, (7468) Anfimov, (53546) 2000 BY6; the (96) Aegle and (618) Elfriede families were also re-reported in M13). These cases highlight the strength of the M14 identification scheme and are included in the family synthesis in Table 2. Some smaller families located inside bigger families (e.g., the (832) Karin family families in the (158) Koronis family, (656) Beagle in (24) Themis) were not reported in M14. In addition, several families were not reported, presumably because the QRL was set too low to detect them. This happens, most notably, in the 2.82–2.96 AU region (i.e., between the 5:2 and 7:3 resonances), where the number density of asteroids is relatively low (see Figures 1 and 9). The notable cases in this region include the (81) Terpsichore, (709) Fringilia, (5567) Durisen, (5614) Yakovlev, (7481) San Marcello and (10811) Lau families. A possible solution to this issue would be, in terms of the M14 identification scheme, to use a separate QRL level for the 2.82–2.96 AU region. Also, several families were split in M14 into several parts. This affects the following families: (8) Flora (split in 4 parts), (31) Euphrosyne (3 parts), (221) Eos (5 parts), (702) Alauda (4 parts), (1400) Tirela (8 parts), (2085) Henan (4 parts), (4203) Brucato (4 parts) (here we only list families that were split to three or more parts in M14).

8. CONCLUSIONS

It is clear from several different arguments that the list of known families must be largely incomplete. For example, most families with an estimated parent body size below $\simeq 100\text{--}200$ km are found to have ages $t_{\text{age}} \lesssim 1$ g.y. (e.g., Brož et al., 2013). In contrast, the rate of impacts in the main belt, and therefore the rate of family-forming events, should have been roughly unchanging with time over the past $\simeq 3.5$ g.y. (and probably raised quite a bit toward the earliest epochs). So, there must be many missing families with the formation ages $t_{\text{age}} > 1$ g.y. (Note 12). These families are difficult to spot today, probably because they have been dispersed by dynamical processes, lost members by collisional grinding, and therefore do not stand out sufficiently well above the dense main-belt background (they are now part of the background).

The significant incompleteness of known families is also indicated by the extrapolation of the number of families detected in the 2.82–2.96 AU zone to the whole main belt. As we hinted on at the end of the last section, the 2.82–2.96 AU zone is sparsely populated such that asteroid families can be more easily detected there. Nearly 20 families with $i_P < 17.5^\circ$ were identified in this region. In comparison, the 2.96–3.3 AU zone, where also $\simeq 20$ families with $i_P < 17.5^\circ$ can be found, is about twice as wide as

the 2.82–2.96 AU zone and contains about twice as many large asteroids. A straightforward conclusion that can be inferred from this comparison, assuming everything else being equal, is that the families in the 2.96–3.3 AU zone are (at least) a factor of ~ 2 incomplete. A similar argument applies to the inner and central belts.

This is actually good news for future generations of planetary scientists, because this field is open for new discoveries. Figuring out how to find the missing asteroid families with $t_{\text{age}} > 1$ g.y. will not be easy. One way forward would be to improve our capability to model the dynamical evolution of main belt asteroids over g.y. timescales, such that we can rewind the clock and track fragments back to their original orbits. The modeling of the Yarkovsky effect could be improved, for example, if we knew the spin states, densities, conductivity, etc., of small main-belt asteroids on individual basis. Another approach would consist in identifying families based on the physical properties of their members. While this method is already in use, mainly thanks to data from the SDSS and WISE, we anticipate that it can be pushed much further, say, with automated spectroscopic surveys, or, in more distant future, with routine sampling missions.

9. NOTES

Note 1 – Alternatively, one can use the frequencies n , g and s (Carruba and Michtchenko, 2007, 2009), where n is the mean orbital frequency and g and s are the (constant) precession frequencies of the proper perihelion longitude ϖ_P and the proper nodal longitude Ω_P , respectively. The use of frequencies, instead of the proper elements, can be helpful for asteroid families near or inside the secular orbital resonances (e.g. the Tina family in the ν_6 resonance; Carruba and Morbidelli, 2011).

Note 2 – Additional methods were developed and/or adapted for specific populations of asteroids such as the ones on the high-inclination and high-eccentricity orbits (Lemaître and Morbidelli, 1994) or in orbital resonances (Morbidelli, 1993; Milani, 1993; Beaugé and Roig, 2001; Brož and Vokrouhlický, 2008; Brož and Rozehnal, 2011).

Note 3 – <http://hamilton.dm.unipi.it/astdys/>

Note 4 – See chapter Bendjoya and Zappalà (2002) in the Asteroids III book for a discussion of other clustering algorithms such as the Wavelet Analysis Method (WAM) and D-criterion. The WAM was shown to produce results that are in a good agreement with those obtained from the HCM (Zappalà et al., 1994). The D-criterion was originally developed to identify meteorite streams (Southwork and Hawkins, 1963). These methods have not been used for the classification of asteroid families in the past decade, and we therefore do not discuss them here.

Note 5 – The SDSS measured flux densities in five bands with effective wavelengths 354, 476, 628, 769, and 925 nm. The WISE mission measured fluxes in four wavelengths (3.4, 4.6, 12 and 22 μm), and combined the measurements with a thermal model to calculate albedos (p_V) and diameters (D). The latest public releases of these catalogs include color or albedo data for over 100,000 main belt asteroids with known orbits, of which about 25,000 have both the color and albedo measurements. The catalogs are available at

www.sdss.org/dr6/products/value_added/index.html and irsa.ipac.caltech.edu/Missions/wise.html.

Note 6 – Most but not all asteroid families are physically homogeneous. The Eos family has the highest diversity of taxonomic classes of any known family (e.g., Mothé-Diniz et al., 2008). This diversity has led to the suggestion that the Eos parent body was partially differentiated. It can also be the source of carbonaceous chondrites (Clark et al., 2009). The Eunomia family may be another case of a relatively heterogeneous family (e.g., Nathues et al., 2005). See Weiss and Elkins-Tanton (2013) for a review.

Note 7 – Dell’Oro et al. (2004) attempted to model observed family shapes by Gaussian ellipsoids. The distribution of $|f|$ obtained in this work was strongly peaked near $\pi/2$, while a more uniform distribution between 0 and π would be expected if different breakups occurred at random orbital phases. This result was attributed to the Yarkovsky effect.

Note 8 – Nesvorný et al. (2008a) found evidence for a large population of V-type asteroids with slightly lower orbital inclinations ($i_P = 3\text{--}4^\circ$) than the Vesta family ($i_P \simeq 5^\circ$). Because these asteroids could not have dynamically evolved from the Vesta family region to their present orbits in ~ 1 g.y., they are presumably fragments excavated from (4) Vesta’s basaltic crust by an earlier impact.

Note 9 – Other asteroid families whose long-term dynamics has been studied in detail, listed here in the alphabetical order, are the Adeona family (affected in e_P and i_P by the 8:3 resonance at 2.705 AU, Carruba et al., 2003), Agnia family (inside the z_1 resonance; Vokrouhlický et al., 2006c), Astrid family (near the border of the 5:2 resonance; Vokrouhlický et al., 2006b), Eunomia family (Carruba et al., 2007b), Euphrosyne family (located in a region with many resonances, including $g - g_6 = 0$, near the inner border of the 2:1 resonance; Carruba et al., 2014), Ergone family (cut in the middle by the z_2 resonance; Vokrouhlický et al., 2006b), Gefion family (affected by various resonances near 2.75 AU, Carruba et al., 2003, Nesvorný et al., 2009), Hilda and Schubart families in the 3:2 resonance with Jupiter (Brož and Vokrouhlický, 2008), Hungaria family (perturbed by $2g - g_5 - g_6 = 0$ and other secular resonances below 1.93 AU; Warner et al. (2009), Milani et al. (2010), also see Galiazzo et al. (2013, 2014) for the contribution of Hungarias to the E-type NEAs and Čuk et al. (2014) for their suggested relation to the aubrite meteorites), Hygiea family (Carruba, 2013; Carruba et al., 2014), Massalia family (the part with $a_P > 2.42$ AU disturbed by the 1:2 resonance with Mars, Vokrouhlický et al., 2006b), Merxia family (spread by the 3J-1S-1 three-body resonance at $a_P = 2.75$ AU; Vokrouhlický et al., 2006b), Padua family (Carruba, 2009a), Pallas family (Carruba et al., 2011), Phocaea family (Carruba, 2009b), Sylvia family ((87) Sylvia has two satellites, possibly related to the impact that produced the Sylvia family, Vokrouhlický et al., 2010), and Tina family (Carruba and Morbidelli, 2011).

Note 10 – <http://sbn.psi.edu/pds/resource/nescvornýfamily.html>

Note 11 – The candidate families are: (929) Algunde, (1296) Andree, (1646) Rosseland, (1942) Jablunka, (2007) McCuskey, (2409) Chapman, (4689) Donn, (6246) Komurotoru and (13698) 1998 KF35 in the inner belt, (46) Hestia, (539) Palmina, (300163) P/2006 VW 139, (3567) Alvema, (7744) 1986 QA1 in the central belt, and (260) Huberta, (928) Hilrun, (2621) Goto, (1113) Katja, (8737) Takehiro in the outer belt. We tentatively moved the (46) Hestia family, previously known as FIN 503, to the family candidate status, because this group is not convincing with the present data. The previously reported groups around (5) Astraea, (1044) Teutonia, (3110) Wagman, (4945) Ikenozenni, (7744) 1986 QA1, (8905) Bankakuko, (25315) 1999 AZ8, (28804) 2000 HC81 seem to align with the $z_1 = g + s - g_6 - s_6 = 0$ resonance and are probably an artifact of the HCM chaining.

Note 12 – The list of known families corresponding to parent bodies with $D > 200$ km, on the other hand, is probably reasonably complete, because the estimated ages of these families appear to be randomly distributed over 4 g.y. (Brož et al., 2013). These largest families can therefore be used to constrain the collisional history of the asteroid belt (see chapter by Bottke et al. in this volume).

Acknowledgments. The work of MB was supported by the Czech Grant Agency (grant no. P209-12-01308S). The work of VC was supported by the São Paulo State (FAPESP grants no. 2014/06762-2) and Brazilian (CNPq grant no. 305453/2011-4) Grant Agencies.

REFERENCES

- Beaugé, C. and Roig, F. (2001) A semi-analytical model for the motion of the Trojan asteroids: proper elements and families. *Icarus*, 153, 391–415.
- Bendjoya, Ph. and Zappalà, V. (2002) Asteroid Family Identification. In: *Asteroids III* (W. Bottke, A. Cellino, P. Paolicchi and R.P. Binzel, Eds.), Univ. Arizona Press and LPI, 613–618.
- Benz, W. and Asphaug, E. (1999) Catastrophic Disruptions Revisited. *Icarus*, 142, 5–20.
- Bottke, W. F., Vokrouhlický, D., Brož, M. et al. (2001) Dynamical Spreading of Asteroid Families by the Yarkovsky Effect. *Science*, 294, 1693–1696.
- Bottke, W. F., Vokrouhlický, D., Rubincam, D. P., and Brož, M. (2002) The Effect of Yarkovsky Thermal Forces on the Dynamical Evolution of Asteroids and Meteoroids. In: *Asteroids III* (W. Bottke, A. Cellino, P. Paolicchi and R.P. Binzel, Eds.), Univ. Arizona Press and LPI, 395–408.
- Bottke, W. F., Durda, D. D., Nesvorný, D. et al. (2005a) The fossilized size distribution of the main asteroid belt. *Icarus*, 175, 111–140.
- Bottke, W. F., Durda, D. D., Nesvorný, D. et al. (2005b) Linking the collisional history of the main asteroid belt to its dynamical excitation and depletion. *Icarus*, 179, 63–94.
- Bottke, W. F., Vokrouhlický, D., Rubincam, D. P., and Nesvorný, D. (2006) The Yarkovsky and Yorpa Effects: Implications for Asteroid Dynamics. *Annual Review of Earth and Planetary Sciences*, 34, 157–191.
- Bottke, W. F., Vokrouhlický, D., and Nesvorný, D. (2007) An asteroid breakup 160 Myr ago as the probable source of the K/T impactor. *Nature*, 449, 48–53.
- Bottke, W. F., Vokrouhlický, D., Walsh, K. J., Delbo, M., Michel, P., Lauretta, D. S., Campins, H., Connolly, H. C., Scheeres, D. J., and Chelsey, S. R. (2015) In search of the source of asteroid (101955) Bennu: Applications of the stochastic YORP model. *Icarus*, 247, 191–217.
- Bottke, W. F. et al. (2015) Collisional evolution of the asteroid belt. In : *Asteroids IV* (P. Michel, F. E. DeMeo, W. Bottke Eds.), Univ. Arizona Press and LPI.
- Bowell, E., Muinonen, K., and Wasserman, L. H. (1994) A Public-Domain Asteroid Orbit Data Base. *Asteroids, Comets, Meteors* 1993, 160, 477.
- Brož, M. and Morbidelli, A. (2013) The Eos family halo. *Icarus*, 223, 844–849.
- Brož, M. and Vokrouhlický, D. (2008) Asteroid families in the first-order resonances with Jupiter. *MNRAS*, 390, 715–732.
- Brož, M., Vokrouhlický, D., Morbidelli, A., Nesvorný, D., and Bottke, W. F. (2011) Did the Hilda collisional family form during the late heavy bombardment? *MNRAS*, 414, 2716–2727.
- Brož, M. and Rozehnal, J. (2011) Eurybates – the only asteroid family among Trojans? *MNRAS*, 414, 565–574.
- Brož, M., Morbidelli, A., Bottke, W. F., et al. (2013) Constraining the cometary flux through the asteroid belt during the late heavy bombardment. *Astron. Astrophys.*, 551, A117.
- Brunetto, R. et al. (2015) Asteroid Surface Alteration by Space Weathering Processes. In : *Asteroids IV* (P. Michel, F. E. DeMeo, W. Bottke Eds.), Univ. Arizona Press and LPI.
- Campbell, M. (1995) Golden Eye, MGM/UA Distribution Company
- Carruba, V. (2009a) The (not so) peculiar case of the Padua family. *MNRAS*, 395, 358–377.
- Carruba, V. (2009b) An analysis of the region of the Phocaea dynamical group. *MNRAS*, 398, 1512–1526.
- Carruba, V. (2010) The stable archipelago in the region of the Pallas and Hansa families. *MNRAS*, 408, 580–600.
- Carruba, V. and Michtchenko, T.A. (2007) A frequency approach to identifying asteroid families. *Astron. Astrophys.*, 75, 1145–

- 1158.
- Carruba, V. and Michtchenko, T. A. (2009) A frequency approach to identifying asteroid families. II. Families interacting with non-linear secular resonances and low-order mean-motion resonances. *Astron. Astrophys.*, **493**, 267–282.
- Carruba, V. and Morbidelli A. (2011) On the first nu(6) anti-aligned librating asteroid family of Tina. *MNRAS*, **412**, 2040–2051.
- Carruba, V., Burns, J. A., Bottke, W. F., and Nesvorný D. (2003) Orbital evolution of the Gefion and Adeona asteroid families: close encounters with massive asteroids and the Yarkovsky effect. *Icarus*, **162**, 308–327.
- Carruba, V., Michtchenko, T. A., Roig, F., Ferraz-Mello, S., and Nesvorný, D. (2005) On the V-type asteroids outside the Vesta family. I. Interplay of nonlinear secular resonances and the Yarkovsky effect: the cases of 956 Elisa and 809 Lundia. *Astron. Astrophys.*, **441**, 819–829.
- Carruba, V., Roig, F., Michtchenko, T. A., Ferraz-Mello, S., and Nesvorný D. (2007a) Modeling close encounters with massive asteroids: a Markovian approach. An application to the Vesta family. *Astron. Astrophys.*, **465**, 315–330.
- Carruba, V., Michtchenko, T. A., and Lazzaro D. (2007b) On the V-type asteroids outside the Vesta family. II. Is (21238) 1995 WV7 a fragment of the long-lost basaltic crust of (15) Eunomia? *Astron. and Astrophys.*, **473**, 967–978.
- Carruba, V., Machuca, J. F., and Gasparino, H. P. (2011) Dynamical erosion of asteroid groups in the region of the Pallas family. *MNRAS*, **412**, 2052–2062.
- Carruba, V., Huaman, M. E., Douwens, S., and Domingos, R. C. (2012) Chaotic diffusion caused by close encounters with several massive asteroids. *Astron. Astrophys.*, **543**, A105.
- Carruba, V., Domingos, R. C., Nesvorný, D., et al. (2013a) A multi-domain approach to asteroid families identification. *MNRAS*, **433**, 2075–2096.
- Carruba, V., Huaman, M. E., Domingos, R. C., and Roig F. (2013b) Chaotic diffusion caused by close encounters with several massive asteroids II: the regions of (10) Hygiea, (2) Pallas, and (31) Euphrosyne, *Astron. Astrophys.*, **550**, A85.
- Carruba, V., Aljbaae, S., and Souami D. (2014), Peculiar Eu-phrosyne, *Astrophys. J.*, **792**, 46–61.
- Cellino, A., Bus, S. J., Doressoundiram, A. and Lazzaro, D. (2002) Spectroscopic Properties of Asteroid Families. In: *Asteroids III* (W. Bottke, A. Cellino, P. Paolicchi and R.P. Binzel, Eds.), Univ. Arizona Press and LPI, 633–643.
- Cellino, A., Dell’Oro, A., and Zappalà, V. (2004) Asteroid families: open problems. *Planetary and Space Science*, **52**, 1075–1086.
- Cellino, A., Dell’Oro, A., and Tedesco, E. F. (2009) Asteroid families: Current situation. *Planetary and Space Science*, **57**, 173–182.
- Cellino, A., Bagnulo, S., Tanga, P., Novaković, B., and Delbó, M. (2014) A successful search for hidden Barbarians in the Watsonia asteroid family. *MNRAS Letters*, **439**, 75–79.
- Cibulková, H., Brož, M., and Benavidez, P. G. (2014) A six-part collisional model of the main asteroid belt. *Icarus*, **241**, 358–372.
- Cimrman, J. (1917) On the literal expansion of the perturbation Hamiltonian and its applicability to the curious assemblages of minor planets. *The Cimrman Bulletin*, **57**, 132–135.
- Clark, B. E., Ockert-Bell, M. E., Cloutis, E. A., Nesvorný, D., Mothé-Diniz, T., and Bus, S. J. (2009) Spectroscopy of K-complex asteroids: Parent bodies of carbonaceous meteorites? *Icarus*, **202**, 119–133.
- Ćuk, M., Gladman, B. J., and Nesvorný, D. (2014) Hungaria asteroid family as the source of aubrite meteorites. *Icarus*, **239**, 154–159.
- Delisle, J.-B. and Laskar, J. (2012) Chaotic diffusion of the Vesta family induced by close encounters with massive asteroids. *Astron. Astrophys.*, **540**, A118.
- Dell’Oro, A., Bigongiari, G., Paolicchi, P., and Cellino, A. (2004) Asteroid families: evidence of ageing of the proper elements. *Icarus*, **169**, 341–356.
- Dell’Oro, A. and Cellino, A. (2007) The random walk of Main Belt asteroids: orbital mobility by non-destructive collisions. *MNRAS*, **380**, 399–416.
- Dermott, S. F., Nicholson, P. D., Burns, J. A., Houck, J. R. (1984) Origin of the solar system dust bands discovered by IRAS. *Nature*, **312**, 505–509.
- Dermott, S. F., Kehoe, T. J. J., Durda, D. D., Grogan, K., Nesvorný, D. (2002) Recent rubble-pile origin of asteroidal solar system dust bands and asteroidal interplanetary dust particles. *Asteroids, Comets, and Meteors*, **500**, 319–322.
- Durda, D. D., Bottke, W. F., Enke, B. L., Merline, W. J., Asphaug, E., Richardson, D. C., and Leinhardt, Z. M. (2004) The formation of asteroid satellites in large impacts: results from numerical simulations. *Icarus*, **170**, 243–257.
- Durda, D. D., Bottke, W. F., Nesvorný, D. et al. (2007) Size-frequency distributions of fragments from SPH/ N-body simulations of asteroid impacts: Comparison with observed asteroid families. *Icarus*, **186**, 498–516.
- Dykhuis, M. and Greenberg, R. (2015) Collisional family structure within the Nysa-Polana complex. *Icarus*, ArXiv e-prints arXiv:1501.04649.
- Dykhuis, M. J., Molnar, L., Van Kooten, S. J., Greenberg, R. (2014) Defining the Flora Family: Orbital properties, reflectance properties and age. *Icarus*, **243**, 111–128.
- Farley, K. A., Vokrouhlický, D., Bottke, W. F., and Nesvorný, D. (2006) A late Miocene dust shower from the break-up of an asteroid in the main belt. *Nature*, **439**, 295–297.
- Florczak, M., Lazzaro, D., and Duffard, R. (2002) Discovering New V-Type Asteroids in the Vicinity of 4 Vesta. *Icarus*, **159**, 178–182.
- Fujiwara, A., Cerroni, P., Davis, D., Ryan, E., and di Martino, M. (1989) Experiments and scaling laws for catastrophic collisions. *Asteroids II*, 240–265.
- Galiazzo, M. A., Bazsó, Á., and Dvorak, R. (2013) Fugitives from the Hungaria region: Close encounters and impacts with terrestrial planets. *Planet. and Space Sci.*, **84**, 5–13.
- Galiazzo, M. A., Bazsó, Á., and Dvorak, R. (2014) The Hungaria Asteroids: close encounters and impacts with terrestrial planets. *Memorie della Societa Astronomica Italiana Supplement*, v.26, p.38.
- Gil-Hutton, R. (2006) Identification of families among highly inclined asteroids. *Icarus*, **183**, 93–100.
- Harris, A. W., Mueller, M., Lisse, C. M., and Cheng, A. F. (2009) A survey of Karin cluster asteroids with the Spitzer Space Telescope. *Icarus*, **199**, 86–96.
- Hirayama, K. (1918) Groups of asteroids probably of common origin. *Astron. J.*, **31**, 185–188.
- Ivezić, Ž., Tabachnik, S., Rafikov, R. et al. (2001) Solar System Objects Observed in the Sloan Digital Sky Survey Commissioning Data. *Astron. J.* **122**, 2749–2784.
- Jenniskens, P. (2015) In *Asteroids IV* (P. Michel, F. E. DeMeo, W. Bottke Eds.), Univ. Arizona Press and LPI.

- Jewitt, D. (2015) The Activated Asteroids. In *Asteroids IV* (P. Michel, F. E. DeMeo, W. Bottke Eds.), Univ. Arizona Press and LPI.
- Knežević, Z., Milani, A., Farinella, P., Froeschle, Ch., and Froeschle, Cl. (1991) Secular resonances from 2 to 50 AU. *Icarus*, 93, 316–330.
- Knežević, Z. and Pavlović, R., (2000) Young Age for the Veritas Asteroid Family Confirmed? *Earth, Moon, and Planets*, 88, 155–166.
- Knežević, Z. and Milani, A. (2000) Synthetic proper elements for outer main belt asteroids. *Celest. Mech. Dyn. Astron.*, 78, 17–46.
- Knežević Z., Lemaître, A. and Milani, A. (2002) The determination of asteroid proper elements. In *Asteroids III* (W. Bottke, A. Cellino, P. Paolicchi and R.P. Binzel, Eds.), Univ. Arizona Press and LPI, 603–612.
- Lemaître A. and Morbidelli A. (1994) Proper elements for highly inclined asteroidal orbits. *Cel. Mech. Dyn. Astron.*, 60, 29–56.
- Low, F. J., Young, E., Beintema, D. A., Gautier, T. N., et al. (1984) Infrared cirrus - New components of the extended infrared emission. *Astrophys. J.*, 278, 19–22.
- Mainzer, A., Grav, T., Masiero, J., et al. (2011) NEOWISE Studies of Spectrophotometrically Classified Asteroids: Preliminary Results. *Astrophys. J.*, 741, 90–115.
- Marchi, S., McSween, H. Y., O'Brien, D. P., et al. (2012) The Violent Collisional History of Asteroid 4 Vesta. *Science*, 336, 690.
- Marchis, F., and 11 colleagues 2014. The Puzzling Mutual Orbit of the Binary Trojan Asteroid (624) Hektor. *Astrophys. J.*, 783, LL37.
- Marsden, B. G. (1980) The Minor Planet Center. *Cel. Mech. Dyn. Astron.*, 22, 63–71.
- Marzari, F., Farinella, P., and Davis, D. R. (1999) Origin, Aging, and Death of Asteroid Families. *Icarus*, 142, 63–77.
- Masiero, J. R., Mainzer, A. K., Grav, T., et al. (2011) Main Belt Asteroids with WISE/NEOWISE. I. Preliminary Albedos and Diameters. *Astrophys. J.*, 741, 68–88.
- Masiero, J. R., Mainzer, A. K., Grav, T., Bauer, J. M., and Jedicke, R. (2012) Revising the Age for the Baptistina Asteroid Family Using WISE/NEOWISE Data. *Astrophys. J.*, 759, 14–28.
- Masiero, J. R., Mainzer, A. K., Bauer, J. M., et al. (2013) Asteroid Family Identification Using the Hierarchical Clustering Method and WISE/NEOWISE Physical Properties. *Astrophys. J.*, 770, 7–29.
- Masiero, J. R. et al. (2015) Physical Properties of Asteroid Families, In *Asteroids IV* (P. Michel, F. E. DeMeo, W. Bottke Eds.), Univ. Arizona Press and LPI.
- Michel, P., Benz, W., Tanga, P., and Richardson, D. C. (2001) Collisions and Gravitational Reaccumulation: Forming Asteroid Families and Satellites. *Science*, 294, 1696–1700.
- Michel, P., Benz, W., and Richardson, D. C. (2003) Disruption of fragmented parent bodies as the origin of asteroid families. *Nature*, 421, 608–611.
- Michel, P., Benz, W., and Richardson, D. C., (2004) Catastrophic disruption of pre-shattered parent bodies. *Icarus*, 168, 420–432.
- Michel, P., Jutzi, M., Richardson, D. C., and Benz, W. (2011) The Asteroid Veritas: An intruder in a family named after it? *Icarus*, 211, 535–545.
- Michel P. et al. (2015) Collisional Formation and Modeling of Families. In : *Asteroids IV* (P. Michel, F. E. DeMeo, W. Bottke Eds.), Univ. Arizona Press and LPI.
- Migliorini, F., Zappalà, V., Vio, R., and Cellino, A. (1995) Interlopers within asteroid families. *Icarus*, 118, 271–291.
- Milani A. (1993) the Trojan asteroid belt: proper elements, chaos, stability and families, *Cel. Mech. Dyn. Astron.*, 57, 59–94.
- Milani, A. and Knežević, Z. (1990) Secular perturbation theory and computation of asteroid proper elements. *Celestial Mechanics*, 49, 347–411.
- Milani, A. and Knežević, Z. (1994) Asteroid proper elements and the dynamical structure of the asteroid main belt. *Icarus* 107, 219–254.
- Milani, A. and Farinella, P. (1994) The age of the Veritas asteroid family deduced by chaotic chronology. *Nature*, 370, 40–42.
- Milani, A., Knežević, Z., Novaković, B., and Cellino, A. (2010) Dynamics of the Hungaria asteroids. *Icarus*, 207, 769–794.
- Milani, A., Cellino, A., Knežević, Z. et al. (2014) Asteroid families classification: Exploiting very large datasets. *Icarus*, 239, 46–73.
- Minton, D. and Malhotra, R. (2009) A record of planet migration in the main asteroid belt. *Nature*, 457, 1109–1111.
- Molnar, L. A. and Haegert, M. J. (2009) Details of Recent Collisions of Asteroids 832 Karin and 158 Koronis. AAS/Division for Planetary Sciences Meeting Abstracts #41, 41, #27.05.
- Morbidelli, A. (1993) Asteroid secular resonant proper elements. *Icarus*, 105, 48–66.
- Morbidelli, A., Brasser, R., Gomes, R., Levison, H. F., Tsiganis, K. (2010) Evidence from the Asteroid Belt for a Violent Past Evolution of Jupiter's Orbit. *Astron. J.*, 140, 1391–1401.
- Mothé-Diniz, T., Roig, F., and Carvano, J. M. (2005) Reanalysis of asteroid families structure through visible spectroscopy. *Icarus*, 174, 54–80.
- Mothé-Diniz, T., Carvano, J. M., Bus, S. J., et al. (2008) Mineralogical analysis of the Eos family from near-infrared spectra. *Icarus*, 195, 277–294.
- Nathues, A., Mottola, S., Kaasalainen, M., and Neukum, G. (2005) Spectral study of the Eunomia asteroid family. I. Eunomia. *Icarus*, 175, 452–463.
- Nesvorný, D. (2010) Nesvorný HCM Asteroid Families V1.0. NASA Planetary Data System, 133.
- Nesvorný, D. (2012) Nesvorný HCM Asteroid Families V2.0. NASA Planetary Data System, 189.
- Nesvorný D. and Morbidelli, A. (1999) An Analytic Model of Three-Body Mean Motion Resonances. *Celestial Mechanics and Dynamical Astronomy*, 71, 243–271.
- Nesvorný D. and Bottke, W. F. (2004) Detection of the Yarkovsky effect for main-belt asteroids. *Icarus*, 170, 324–342.
- Nesvorný, D. and Vokrouhlický, D. (2006) New Candidates for Recent Asteroid Breakups. *Astron. J.*, 132, 1950–1958.
- Nesvorný D., Bottke, W. F., Dones, L., and Levison, H. F. (2002a) The recent breakup of an asteroid in the main-belt region. *Nature*, 417, 720–771.
- Nesvorný, D., Morbidelli, A., Vokrouhlický, D., Bottke, W. F., and Brož, M. (2002b) The Flora Family: A Case of the Dynamically Dispersed Collisional Swarm? *Icarus*, 157, 155–172.
- Nesvorný, D., Ferraz-Mello, S., Holman, M., and Morbidelli, A. (2002c) Regular and Chaotic Dynamics in the Mean-Motion Resonances: Implications for the Structure and Evolution of the Asteroid Belt. In: *Asteroids III* (W. Bottke, A. Cellino, P. Paolicchi and R.P. Binzel, Eds.), Univ. Arizona Press and LPI, 379–394.
- Nesvorný D., Bottke, W. F., Levison, H. F., and Dones, L. (2003) Recent Origin of the Solar System Dust Bands. *Astrophys. J.*, 591, 486–497.

- Nesvorný D., Jedicke, R., Whiteley, R. J., and Ivezić, Ž. (2005) Evidence for asteroid space weathering from the Sloan Digital Sky Survey. *Icarus*, 173, 132–152.
- Nesvorný, D., Enke, B. L., Bottke, W. F., Durda, D. D., Asphaug, E., and Richardson, D. C. (2006a) Karin cluster formation by asteroid impact. *Icarus*, 183, 296–311.
- Nesvorný, D., Bottke, W. F., Vokrouhlický, D., Morbidelli, A., and Jedicke, R. (2006b) Asteroid families. *Asteroids, Comets, Meteors*, 229, 289–299.
- Nesvorný, D., Vokrouhlický, D., and Bottke, W.F. (2006c) The Breakup of a Main-Belt Asteroid 450 Thousand Years Ago. *Science*, 312, 1490.
- Nesvorný, D., Roig, F., Gladman, B., et al. (2008a) Fugitives from the Vesta family. *Icarus*, 183, 85–95.
- Nesvorný, D., Bottke, W. F., Vokrouhlický, D. et al. (2008b) Origin of the Near-Ecliptic Circumsolar Dust Band. *Astrophys. J.*, 679, 143–146.
- Nesvorný, D., Vokrouhlický, D., Morbidelli, A., and Bottke, W. F. (2009) Asteroidal source of L chondrite meteorites. *Icarus*, 200, 698–701.
- Novaković, B. (2010) Portrait of Theobalda as a young asteroid family. *MNRAS*, 407, 1477–1486.
- Novaković, B., Tsiganis, K., and Knežević, Z. (2010) Dynamical portrait of the Lixiaohua asteroid family. *Celestial Mechanics and Dynamical Astronomy*, 107, 35–49.
- Novaković, B., Tsiganis, K., and Knežević, Z. (2010) Chaotic transport and chronology of complex asteroid families. *MNRAS*, 402, 1263–1272.
- Novaković, B., Cellino, A., and Knežević, Z. (2011) Families among high-inclination asteroids. *Icarus*, 216, 69–81.
- Novaković, B., Dell’Oro, A., Cellino, A., and Knežević, Z. (2012a) Recent collisional jet from a primitive asteroid. *MNRAS*, 425, 338–346.
- Novaković, B., Hsieh, H. H., and Cellino, A. (2012b) P/2006 VW139: a main-belt comet born in an asteroid collision? *MNRAS*, 424, 1432–1441.
- Novaković, B., Hsieh, H.H., Cellino, A., Michel, M., and Pedanum, M. (2014) Discovery of a young asteroid cluster associated with P/2012 F5 (Gibbs). *Icarus*, 231, 300–309.
- Parker, A., Ivezić, Ž., Jurić, M., et al. (2008) The size distributions of asteroid families in the SDSS Moving Object Catalog 4. *Icarus*, 198, 138–155.
- Reddy, V., Carvano, J. M., Lazzaro, D. et al. (2011) Mineralogical characterization of Baptistina Asteroid Family: Implications for K/T impactor source. *Icarus*, 216, 184–197.
- Rozehnal, J. and Brož, M. (2013) Jovian Trojans: Orbital structures versus the WISE data. American Astronomical Society, DPS meeting #45, #112.12.
- Rožek, A., Breiter, S., and Jopek, T. J. (2011) Orbital similarity functions - application to asteroid pairs. *MNRAS*, 412, 987–994.
- Rubincam, D. P. (1995) Asteroid orbit evolution due to thermal drag. *Journal of Geophys. Research*, 100, 1585–1594.
- Rubincam, D. P. (2000) Radiative Spin-up and Spin-down of Small Asteroids. *Icarus*, 148, 2–11.
- Roig, F., Ribeiro, A. O., and Gil-Hutton, R. (2008) Taxonomy of asteroid families among the Jupiter Trojans: comparison between spectroscopic data and the Sloan Digital Sky Survey colors. *Astron. Astrophys.*, 483, 911–931.
- Southworth, R. B. and Hawkins, G. S. (1963) Statistics of meteor streams. *Smithsonian Contributions to Astrophysics*, 7, 261.
- Tsiganis, K., Knežević, Z., and Varvoglis, H. (2007) Reconstructing the orbital history of the Veritas family. *Icarus*, 186 484–497.
- Usui, F., Kasuga, T., Hasegawa, S., et al. (2013) Albedo Properties of Main Belt Asteroids Based on the All-Sky Survey of the Infrared Astronomical Satellite AKARI. *Astrophys. J.*, 762, 56–70.
- Vernazza, P., Binzel, R. P., Thomas, C. A., et al. (2008) Compositional differences between meteorites and near-Earth asteroids. *Nature*, 454, 858–860.
- Vokrouhlický, D. and Nesvorný, D. (2008) Pairs of Asteroids Probably of a Common Origin. *Astron. J.*, 136, 280–290.
- Vokrouhlický, D., and Nesvorný, D. (2011) Half-brothers in the Schulhof Family? *Astron. J.*, 142, 26–34.
- Vokrouhlický, D., Brož, M., Morbidelli, A., et al. (2006a) Yarkovsky footprints in the Eos family. *Icarus*, 182, 92–117.
- Vokrouhlický, D., Brož, M., Bottke, W. F., Nesvorný, D., and Morbidelli, A. (2006b) Yarkovsky/YORP chronology of asteroid families. *Icarus*, 182, 118–142.
- Vokrouhlický, D., Brož, M., Bottke, W. F., Nesvorný, D., and Morbidelli, A. (2006c) The peculiar case of the Agnia asteroid family *Icarus*, 183, 349–361.
- Vokrouhlický, D. and Nesvorný, D. (2009) The Common Roots of Asteroids (6070) Rheinland and (54827) 2001 NQ8. *Astron. J.*, 137, 111–117.
- Vokrouhlický, D., Durech, J., Michalowski, T., et al. (2009) Datura family: the 2009 update. *Astron. Astrophys.*, 507, 495–504.
- Vokrouhlický, D., Nesvorný, D., Bottke, W. F., and Morbidelli, A. (2010) Collisionally Born Family About 87 Sylvia. *Astron. J.*, 139, 2148–2158.
- Vokrouhlický, D., Ďurech, J., Polishook, D., et al. (2011) Spin Vector and Shape of (6070) Rheinland and Their Implications. *Astron. J.*, 142, 159–167.
- Vokrouhlický, D. et al. (2015) Yarkovsky and YORP. In *Asteroids IV* (P. Michel, F. E. DeMeo, W. Bottke Eds.), Univ. Arizona Press and LPI.
- Walsh, K. J., Delbo, M., Bottke, W. F., et al. (2013) Introducing the Eulalia and new Polana asteroid families: Re-assessing primitive asteroid families in the inner Main Belt. *Icarus*, 225, 283–297.
- Warner, B. D., Harris, A. W., Vokrouhlický, D., et al. (2009) Analysis of the Hungaria asteroid population. *Icarus*, 204, 172–182.
- Weiss, B. P., Elkins-Tanton, L. T. (2013) Differentiated Planetary and the Parent Bodies of Chondrites. *Annual Review of Earth and Planetary Sciences*, 41, 529–560.
- Willman, M., Jedicke, R., Nesvorný, D., Moskovitz, N., Ivezić, Ž., and Fevig, R. (2008) Redetermination of the space weathering rate using spectra of Iannini asteroid family members. *Icarus*, 195, 663–673.
- Wisdom, J. (1982) The origin of the Kirkwood gaps - A mapping for asteroidal motion near the 3/1 commensurability. *Astron. J.*, 87, 577–593.
- Zappalà, V., Cellino, A., Farinella, P., and Knežević, Z. (1990) Asteroid families. I - Identification by hierarchical clustering and reliability assessment. *Astron. J.*, 100, 2030–2046.
- Zappalà, V., Cellino, A., Farinella, P., and Milani, A. (1994) Asteroid families. 2: Extension to unnumbered multiopposition asteroids. *Astron. J.*, 107, 772–801.
- Zappalà, V., Cellino, A., dell’Oro, A., Paolicchi, P. (2002) Physical and Dynamical Properties of Asteroid Families. In *Asteroids III* (W. Bottke, A. Cellino, P. Paolicchi and R.P. Binzel, Eds.), Univ. Arizona Press and LPI, 619–631.

Table 2: Notable asteroid families. The columns are the: (1) Family Identification Number (FIN), (2) family name, (3) cutoff distance (d_{cut} ; asterisk denotes d_{cut} used on a subset of asteroids with $p_V < 0.15$), (4) number of family members identified with d_{cut} , (5) largest member(s) in the family (either the number designation of the largest member(s), in parenthesis, if different from the asteroid after which the family is named, or the estimated diameter of the largest member, D_{LM}), (6) diameter of a sphere with volume equivalent to that of all fragments (D_{frag}), (7) C_0 parameter defined in Section 4, (8) taxonomic type, (9) mean geometric albedo from WISE (p_V), and (10) various references and notes. We do not report t_{age} here but note that t_{age} can be estimated from C_0 given in column 7 and Eq. (2). See <http://sirrah.troja.mff.cuni.cz/~mira/mp/fams/> for additional information on asteroid families (Brož et al., 2013).

FIN	Family Name	d_{cut} (m s ⁻¹)	# of mem.	D_{LM} (km)	D_{frag} (km)	C_0 (10 ⁻⁴ AU)	Tax. Type	p_V	References and Notes
<i>Hungarias, Hildas and Jupiter Trojans</i>									
001	153 Hilda	130	409	164	—	—	C	0.04	Brož et al. (2011)
002	1911 Schubart	60	352	80	91	—	C	0.03	Brož and Vokrouhlický (2008)
003	434 Hungaria	100	2965	10	24	0.3 ± 0.1	E	0.35	Warner et al. (2010), Milani et al. (2011)
004	624 Hector	50	12	231	—	—	—	—	satellite, Marchis et al. (2014), Rozehnal and Brož (2014)
005	3548 Eurybates	50	218	68	87	—	CP	0.06	Roig et al. (2008), Brož and Rozehnal (2011)
006	9799 1996 RJ	60	7	72	26	—	—	0.06	Rozehnal and Brož (2014)
007	James Bond	∞	1	(himself)	—	—	ASP	variable	Campbell et al. (1995)
008	20961 Arkesilaos	50	37	—	—	—	—	—	Rozehnal and Brož (2014)
009	4709 Ennomos	100	30	(1867,4709)	—	—	—	0.06	Rozehnal and Brož (2014)
010	247341 2001 UV209	100	13	—	—	—	—	0.09	Rozehnal and Brož (2014)
<i>Inner Main Belt, 2.0 < a < 2.5 AU, i < 17.5°</i>									
401	4 Vesta	50	15252	525	50	1.5 ± 0.5	V	0.35	source of HEDs, two overlapping families?
402	8 Flora	60	13786	(8,254)	—	2.5 ± 0.5	S	0.30	dispersed, source of LL NEAs, Dykhuis et al. (2014)
403	298 Baptistina	45	2500	21	—	0.25 ± 0.05	X	0.16	related to K/T impact? Bottke et al. (2007)
404	20 Massalia	55	6424	132	27	0.25 ± 0.05	S	0.22	Vokrouhlický et al. (2006b)
405	44 Nysa-Polana	50	19073	(135,142,495)	—	1.0 ± 0.5	SFC	0.28/0.06	Walsh et al. (2013), Dykhuis and Greenberg (2015)
406	163 Erigone	50	1776	72	46	0.2 ± 0.05	CX	0.06	Vokrouhlický et al. (2006b)
407	302 Clarissa	55	179	34	15	0.05 ± 0.01	X	0.05	compact with ears, cratering
408	752 Sulamitis	55	303	61	35	0.3 ± 0.1	C	0.04	
409	1892 Lucienne	100	142	11	11	0.15 ± 0.05	S	0.22	
410	27 Euterpe	65	474	110	16	0.50 ± 0.25	S	0.26	
411	1270 Datura	10	6	8	3	—	S	0.21	Nesvorný et al. (2006c)
412	21509 Lucascavin	10	3	—	—	—	S	—	Nesvorný and Vokrouhlický (2006)
413	84 Klio	130*	330	78	33	0.75 ± 0.25	C	0.07	interloper 12?, Masiero et al. (2013)
414	623 Chimaera	120	108	43	21	0.3 ± 0.1	CX	0.06	Masiero et al. (2013)
415	313 Chaldaea	130*	132	(313,1715)	—	1.0 ± 0.5	C	0.07	1715 in Masiero et al. (2013)
416	329 Svea	150	48	70	21	0.3 ± 0.1	CX	0.06	new, near 3:1
417	108138 2001 GB11	20	9	—	—	—	—	—	new, compact
<i>Inner Main Belt, 2.0 < a < 2.5 AU, i > 17°</i>									
701	25 Phocaea	150	1989	(25,587)	—	2.0 ± 1.0	S	0.22	Carruba (2009b), Carruba et al. (2010)

Table 2: Continued.

FIN	Family Name	d_{cut} (m s ⁻¹)	# of mem.	D_{LM} (km)	D_{frag} (km)	C_0 (10 ⁻⁴ AU)	Tax. Type	p_V	References and Notes
<i>Central Main Belt, 2.5 < a < 2.82 AU, i < 17.5°</i>									
501	3 Juno	55	1684	231	25	0.5 ± 0.2	S	0.25	cratering, relation to H chondrites?
502	15 Eunomia	50	5670	256	100	2.0 ± 0.7	S	0.19	continues beyond 5:2?
503	–	–	–	–	–	–	–	–	46 Hestia moved to candidates
504	128 Nemesis	50	1302	178	50	0.25 ± 0.05	C	0.05	3827 in Milani et al. (2014), 125 in Cellino et al. (2002)
505	145 Adeona	50	2236	141	78	0.7 ± 0.3	C	0.07	
506	170 Maria	60	2940	(472,170)	–	2.0 ± 1.0	S	0.25	(472) Roma in Masiero et al. (2013)
507	363 Padua	45	1087	91	48	0.5 ± 0.2	X	0.10	Carruba (2009a), also known as the (110) Lydia family
508	396 Aeolia	20	296	46	13	0.075 ± 0.025	X	0.17	compact, young?
509	410 Chloris	80	424	107	56	0.75 ± 0.25	C	0.06	eroded
510	569 Misa	50	702	65	57	0.5 ± 0.2	C	0.03	V-shaped subfamily inside
511	606 Brangane	55	195	36	18	0.04 ± 0.01	S	0.10	compact, 606 offset, interloper?
512	668 Dora	45	1259	(1734,668)	–	–	C	0.05	668 offset, 1734 in Masiero et al. (2013), V-shaped subfamily
513	808 Merxia	55	1215	34	28	0.3 ± 0.1	S	0.23	Vokrouhlický et al. (2006b)
514	847 Agnia	30	2125	(847,3395)	–	0.15 ± 0.05	S	0.18	z_1 resonance, Vokrouhlický et al. (2006c)
515	1128 Astrid	60	489	42	29	0.12 ± 0.02	C	0.08	Vokrouhlický et al. (2006b)
516	1272 Gefion	50	2547	(2595,1272)	–	0.8 ± 0.3	S	0.20	source of L chondrites? Nesvorný et al. (2009), also known as 93 and 2595
517	3815 Konig	55	354	22	34	0.06 ± 0.03	CX	0.04	compact, young? Nesvorný et al. (2003), 342 and 1639 offset
518	1644 Rafita	70	1295	(1658,1587)	–	0.5 ± 0.2	S	0.25	1644 probably interloper
519	1726 Hoffmeister	45	1819	(272,1726)	–	0.20 ± 0.05	CF	0.04	(272) Antonia in Masiero et al. (2013), but 272 offset
520	4652 Iannini	25	150	5	10	–	S	0.32	1547 offset, compact, Nesvorný et al. (2003)
521	7353 Kazuya	50	44	11	10	–	S	0.21	small clump
522	173 Ino	50	463	161	21	0.5 ± 0.2	S	0.24	also known as 18466, large and dark 173 is probably interloper, ears?
523	14627 Emilkowalski	10	4	7	3	–	S	0.20	Nesvorný and Vokrouhlický (2006)
524	16598 1992 YC2	10	3	–	–	–	S	–	Nesvorný and Vokrouhlický (2006)
525	2384 Schulhof	10	6	12	4	–	S	0.27	Vokrouhlický and Nesvorný (2011)
526	53546 2000 BY6	40	58	8	18	–	C	0.06	Milani et al. (2014)
527	5438 Lorre	10	2	30	–	–	C	0.05	Novaković et al. (2012)
528	2782 Leonidas	50	135	(4793,2782)	–	–	CX	0.07	new, related to 144?
529	144 Vibilia	100*	180	142	–	–	C	0.06	Masiero et al. (2013), PDS list identical to 2782
530	322 Phaeo	100*	146	72	31	0.3 ± 0.1	X	0.06	Cellino et al. (2002), joins (2669) Shostakovich
531	2262 Mitidika	100*	653	(404,5079)	–	–	C	0.06	dispersed, 404 offset, 2262 has $p_V = 0.21$
532	2085 Henan	50	1872	18	32	0.75 ± 0.25	L	0.20	2085 offset in i_P , 4 families in Milani et al. (2014)
533	1668 Hanna	60	280	22	32	0.2 ± 0.1	CX	0.05	Masiero et al. (2013)
534	3811 Karma	60	124	26	24	0.25 ± 0.05	CX	0.05	Milani et al. (2014)

Table 2: Continued.

FIN	Family Name	d_{cut} (m s $^{-1}$)	# of mem.	D_{LM} (km)	D_{frag} (km)	C_0 (10 $^{-4}$ AU)	Tax. Type	p_V	References and Notes
<i>Central Main Belt, 2.5 < a < 2.82 AU, i < 17.5°</i>									
535	2732 Witt	45	1816	11	25	0.75 ± 0.25	S	0.26	relation to the Charis family beyond 5:2? 10955 and 19466 in Milani et al.
536	2344 Xizang	65	275	17	20	0.3 ± 0.1	—	0.12	Milani et al. (2014), includes 396
537	729 Watsonia	130	99	52	38	—	L	0.13	Cellino et al. (2014)
538	3152 Jones	40	22	37	11	—	T	0.05	new, compact, diagonal in (a_P, e_P)
539	369 Aeria	90	272	75	17	0.3 ± 0.1	X	0.17	new, part above 2.6778 AU down in i_P
540	89 Julia	70	33	147	6	—	S	0.19	new, compact
541	1484 Postrema	100	108	47	—	—	CX	0.05	new, large 387,547,599?
<i>Central Main Belt, 2.5 < a < 2.82 AU, i > 17.5°</i>									
801	2 Pallas	350	128	513	40	—	B	0.16	Carruba et al. (2010, 2012), part beyond 5:2
802	148 Gallia	200	182	81	19	0.5 ± 0.1	S	0.17	large interlopers
803	480 Hansa	200	1094	56	62	—	S	0.26	2 families in Milani et al. (2014)
804	686 Gersuind	120	415	49	36	—	S	0.15	2 families in Milani et al. (2014)
805	945 Barcelona	150	306	27	19	0.25 ± 0.05	S	0.25	2 families in Milani et al. (2014)
806	1222 Tina	200	96	26	10	0.10 ± 0.05	X	0.34	in the $g - g_6 = 0$ resonance, Carruba and Morbidelli (2011)
807	4203 Brucato	200	342	18	44	0.5 ± 0.2	CX	0.06	1263 interloper? Carruba (2010), 4 families in Milani et al. (2014)
<i>Outer Main Belt, 2.82 < a < 3.7 AU, i < 17°</i>									
601	10 Hygiea	60	4854	428	—	—	CB	0.06	Carruba et al. (2014)
602	24 Themis	60	4782	177	230	2.5 ± 1.0	C	0.07	includes 656 Beagle, Nesvorný et al. (2008b)
603	87 Sylvia	130	255	263	—	—	X	0.05	Vokrouhlický et al. (2010)
604	137 Meliboea	85	444	(511,137)	—	—	C	0.05	(511) Davida in Masiero et al. (2013)
605	158 Koronis	45	5949	(208,158,462)	—	2.0 ± 1.0	S	0.15	(208) Lacrimosa in Masiero et al. (2013)
606	221 Eos	45	9789	(221,579,639)	—	1.5 ± 0.5	K	0.13	Vokrouhlický et al. (2006a), Brož and Morbidelli (2013)
607	283 Emma	40	76	122	56	0.3 ± 0.1	C	0.05	affected by the z_1 resonance?
608	293 Brasilia	50	579	(3985)	—	0.20 ± 0.05	X	0.18	293 interloper?, also known as (1521) Sejnajoki, Nesvorný et al. (2003)
609	490 Veritas	30	1294	113	78	0.2 ± 0.1	CPD	0.07	see Section 3
610	832 Karin	10	541	17	16	0.03 ± 0.01	S	0.21	see Section 3, Harris et al. (2009)
611	845 Naema	35	301	61	37	0.20 ± 0.05	C	0.08	
612	1400 Tirela	50	1395	(1040,1400)	—	0.75 ± 0.25	S	0.07	8 families in Milani et al. (2014)
613	3556 Lixiaohua	45	756	(3330,3556)	—	0.25 ± 0.05	CX	0.04	3330 offset, Novaković et al. (2010)
614	9506 Telramund	45	468	(179,9506)	—	—	S	0.22	(179) Klytaemnestra in Masiero et al. and Milani et al.
615	18405 FY12	50	104	9	14	0.08 ± 0.03	CX	0.17	

Table 2: Continued.

FIN	Family Name	d_{cut} (m s ⁻¹)	# of mem.	D_{LM} (km)	D_{frag} (km)	C_0 (10 ⁻⁴ AU)	Tax. Type	p_{v}	References and Notes
<i>Outer Main Belt, 2.82 < a < 3.7 AU, i < 17.5°</i>									
616	627 Charis	80	808	50	45	—	C	0.08	16286 in Milani et al. (2014), related to Witt family?
617	778 Theobalda	60	376	66	50	—	CX	0.06	778 offset, Novaković et al. (2010)
618	1189 Terentia	60	79	63	18	0.13 ± 0.03	C	0.07	
619	10811 Lau	120	56	8	6	0.075 ± 0.025	S	0.27	36824 interloper?
620	656 Beagle	25	148	54	28	0.07 ± 0.03	C	0.09	656 and 90 offset, Nesvorný et al. (2008b)
621	158 Koronis(2)	8	246	34	13	0.010 ± 0.005	S	0.14	young, Molnar and Haegert (2009)
622	81 Terpsichore	120	138	123	27	0.50 ± 0.25	C	0.05	
623	709 Fringilla	150	134	96	55	—	X	0.05	large 1191
624	5567 Durisen	100	27	34	23	—	X	0.04	
625	5614 Yakovlev	120	67	13	23	0.15 ± 0.05	C	0.05	
626	7481 San Marcello	100	144	(3978,7489)	—	—	X	0.19	also known as 12573
627	15454 1998 YB3	80	38	(3156,15454)	—	0.10 ± 0.05	CX	0.05	
628	15477 1999 CG1	95	248	—	—	—	S	0.10	
629	36256 1999 XT17	70	58	(15610,36256)	—	0.25 ± 0.05	S	0.21	several large bodies
630	96 Aegle	50	99	165	38	—	CX	0.07	Masiero et al. and Milani et al.
631	375 Ursula	70	1466	(1306,375)	—	—	CX	0.06	Masiero et al. and Milani et al.
632	618 Elfriede	40	63	122	26	—	C	0.05	compact, recent?
633	918 Itha	100	54	21	35	—	S	0.23	dispersed, many sizable members
634	3438 Inarradas	80	38	25	33	—	CX	0.07	Milani et al. (2014)
635	7468 Anfimov	60	58	10	14	—	S	0.16	Milani et al. (2014)
636	1332 Marconia	30	34	50	16	—	CX	0.05	new
637	106302 2000 UJ87	60	64	7	15	—	CX	0.05	new, large 132999
638	589 Croatia	45	93	92	31	0.5 ± 0.2	X	0.07	new, 21885 in Milani et al. (2014)
639	926 Imhilde	70	43	50	18	0.2 ± 0.1	CX	0.05	new
640	P/2012 F5 (Gibbs)	10	8	—	—	—	—	—	Novaković et al. (2014)
641	816 Juliana	80	76	68	39	—	CX	0.05	Masiero et al. (2013)
<i>Outer Main Belt, 2.82 < a < 3.5 AU, i > 17.5°</i>									
901	31 Euphrosyne	120	2035	276	130	—	C	0.06	Carruba et al. (2014), 3 families in Milani et al. (2014)
902	702 Alauda	120	1294	191	—	2.5 ± 1.0	B	0.07	276 and 1901 offset, 4 families in Milani et al. (2014)
903	909 Ulla	120	26	113	28	—	X	0.05	
904	1303 Luthera	50	163	87	56	—	X	0.04	also known as (781) Kartivelia
905	780 Armenia	50	40	98	22	—	C	0.05	compact